NASA CONTRACTOR REPORT

NASA CR-2380

NASA CR-2380

SENSITIVITY ANALYSIS OF TORSIONAL VIBRATION CHARACTERISTICS OF HELICOPTER ROTOR BLADES

Part II - Aerodynamics and Sensitivity Analysis

by Theodore Bratanow and Akin Ecer

NATIONAL AERONAUTICS AND SPACE ADMINISTRATION • WASHINGTON, D. C. • MARCH 1974

1. Report No. NASA CR-2380	2. Government Accession No.	3. Recipient's Catalog No.
4. Title and Subtitle SENSITIVITY ANALYSIS OF TORSIONAL VIBRATION CHARACTERISTICS OF HELICOPTER ROTOR BLADES - PART II. AERODYNAMICS AND SENSITIVITY ANALYSIS		5. Report Date MARCH 1974
		6. Performing Organization Code
7. Author(s) THEODORE BRATANOW AND AKIN ECER		8. Performing Organization Report No.
		10. Work Unit No.
9. Performing Organization Name and Address UNIVERSITY OF WISCONSIN - MILWAUKEE MILWAUKEE, WISCONSIN		11. Contract or Grant No. NGR 50-007-001
		13. Type of Report and Period Covered CONTRACTOR REPORT
12. Sponsoring Agency Name and Address NATIONAL AERONAUTICS AND SPACE ADMINISTRATION WASHINGTON, D.C. 20546		14. Sponsoring Agency Code

15. Supplementary Notes

TOPICAL REPORT

16. Abstract

A THEORETICAL INVESTIGATION OF DYNAMIC RESPONSE CHARACTERISTICS OF ROTOR BLADES WAS CARRIED OUT WITH SPECIAL EMPHASIS ON TORSIONAL DEGREES-OF-FREEDOM. COUPLED EQUATIONS OF MOTION FOR FLAPWISE BENDING AND TORSION WERE FORMULATED AT VARYING AZIMUTH POSITIONS FOR ROTOR BLADES WITH NONCOLLINEAR AERODYNAMIC, ELASTIC AND MASS AXES. BOTH STRUCTURAL AND AERODYNAMIC MASS, DAMPING AND STIFFNESS COEFFICIENTS WERE INCLUDED. THE VIBRATIONS OF A SAMPLE BLADE AT DIFFERENT FLIGHT CONDITIONS WERE INVESTIGATED FROM THESE EQUATIONS. THE OBTAINED NUMERICAL RESULTS WERE ILLUSTRATED.

THE SENSITIVITY OF OVERALL BLADE VIBRATION CHARACTERISTICS TO TORSIONAL OSCILLATIONS WAS ALSO INVESTIGATED FROM THE EQUATIONS OF MOTION FOR THE SAMPLE BLADE. THE ILLUSTRATED RESULTS SHOW THE IMPORTANCE OF TORSIONAL DEGREES-OF-FREEDOM IN ROTOR BLADE ANALYSIS. VARIOUS POSSIBILITIES OF IMPROVING THE OVERALL RESPONSE BY TUNING BLADE GEOMETRIC, STRUCTURAL AND AERODYNAMIC CHARACTERISTICS ARE DISCUSSED.

17. Key Words (Suggested by Author(s)) ROTOR BLADE DYANMICS AERODYNAMIC LOADS TORSIONAL OSCILLATIONS COUPLED RESPONSE	18. Distribution Statement UNCLASSIFIED - UNLIMITED Cat. 32
19. Security Classif. (of this report) UNCLASSIFIED	20. Security Classif. (of this page) UNCLASSIFIED	21. No. of Pages 62	22. Price $3.50

Page Intentionally Left Blank

CONTENTS

TABLES

ILLUSTRATIONS

SENSITIVITY ANALYSIS OF TORSIONAL VIBRATION
CHARACTERISTICS OF HELICOPTER ROTOR BLADES

Part II. AERODYNAMICS AND SENSITIVITY ANALYSIS

By Theodore Bratanow* and Akin Ecer**
University of Wisconsin-Milwaukee

SUMMARY

A theoretical investigation of dynamic response characteristics of rotor blades was carried out with special emphasis on torsional degrees-of-freedom. The major steps of the analysis are:

. determining the aerodynamic loads on the blade for selected forward flight conditions

. application of a numerical method for determining the sensitivity of blade vibration characteristics with respect to structural, geometric and aerodynamic properties and flight conditions.

Coupled equations of motion for flapwise bending and torsion were formulated at varying azimuth positions for rotor blades with noncollinear aerodynamic, elastic and mass axes. Both structural and aerodynamic mass, damping and stiffness coefficients were included. The vibrations of a sample blade at different flight conditions were investigated from these equations. The obtained numerical results were illustrated.

The sensitivity of overall blade vibration characteristics to torsional oscillations was also investigated from the equations of motion for the sample blade. The illustrated results show the importance of torsional degrees-of-freedom in rotor blade analysis. Various possibilities of improving the overall response by tuning blade geometric, structural and aerodynamic characteristics are discussed.

* Professor, ** Assistant Professor, Department of Mechanics, College of Engineering and Applied Science.

INTRODUCTION

The objectives of the conducted investigation were to determine the variation of torsional oscillations and their effect in forward flight on blade dynamic response characteristics and to analyze the sensitivity of torsional oscillations to blade aerodynamic, structural and geometric properties. In the first report [1], the structural aspects of the analysis were presented. In this report the aerodynamic characteristics of rotor blades are defined for varying forward flight conditions. The unsteady effects due to the pitching motion of the blade were determined from two-dimensional airfoil theory [2]. The aerodynamic loading in each of the structural vibration modes was determined for different flight conditions and then the aerodynamic stiffness and damping coefficients were calculated. These coefficients were compared with structural stiffness and damping coefficients for varying azimuth positions. Then the structural and aerodynamic coefficients were combined for a complete, coupled vibration analysis in forward flight. The sensitivity of the torsional vibrations in forward flight to structural and geometric properties of the sample blade was investigated. The effects of the variations of mass, elastic and aerodynamic axes of the sample blade were illustrated for various flight conditions.

SYMBOLS

a   lift curve slope for forward flow

a'   lift curve slope for reverse flow

a_{ij} generalized aerodynamic mass coefficient

b_{ij} generalized aerodynamic damping coefficient

B   tip loss factor

c   blade chord-width, m.

c_{ij} generalized aerodynamic stiffness coefficient

C_L lift coefficient

$C_{\theta i}$ generalized control moment stiffness in torsion

$\underline{D}$ damping matrix

$f_i(t)$ generalized external load function in each mode, N

$\underline{F}(t)$ generalized external load function, N

$F_i(\psi)$ generalized force in bending, N

$G_i(\psi)$ generalized control moment in torsion, N-m

h vertical displacement of the blade at the elastic center, m.

$\overline{h}_i$ eigenfunction corresponding to the bending displacement component of $\underline{p}_i$, m.

$\underline{K}$ stiffness matrix

L lift generated by a blade, N

L_R lift generated by a blade in reverse flow, N

$L_{ei}(\psi)$ forcing function component for lift, N

m_{ih} generalized coupled torsional stiffness in bending, N-m^2

$M_{ei}(\psi)$ forcing function component for moment, N-m

M_F a feathering moment, N-m

$\underline{M}$ mass matrix

$\underline{p}_i$ eigenvector of the structural system

p_{ij} generalized torsional damping in torsion, N-sec./rad

P_{ij} generalized bending damping in bending, N-sec./m

q_{ij} generalized torsional stiffness in torsion, N/rad

Q_{ij} generalized bending stiffness in bending, N/m

r distance of rotor blade element from center of rotation, m.

$\underline{r}$ coupled displacement vector, m.

R rotor radius, m.

R_{ki} generalized coupled bending stiffness in torsion, N/m

S_{ki} generalized coupled bending damping in torsion, N-sec./rad

t time (sec.)

U_p normal component of the resultant velocity at a blade element, m/sec.

U_t tangential component of the resultant velocity at a blade element, m/sec.

v_i	induced velocity, m/sec.
V	forward velocity, m/sec.
x_θ	eccentricity between the elastic and mass center, m.
X_i	generalized bending deflection at blade tip, m.
Y_i	generalized torsional rotation at blade tip, rad
Z_i	generalized displacement in a coupled mode, m.
α_i	generalized structural mass coefficient
α_r	blade element angle of attack, rad
β	blade flapping angle at particular azimuth position, rad
$\bar{\beta}_i$	eigenfunction corresponding to the bending rotation component of p_i, rad
β_i	generalized structural damping coefficient, N-sec./m
γ_i	generalized structural stiffness coefficient, N/m
ϵ	an angle defining reverse flow region, rad
θ	pitch change due to blade torsion, rad
θ_c	lateral cyclic pitch control input, rad
$\bar{\theta}_i$	eigenfunctions corresponding to the torsional rotation component of p_i, rad
θ_o	collective pitch, rad
θ_s	longitudinal cyclic pitch control input, rad
θ_p	pitch angle of a blade element without considering torsion, rad
θ_1	built-in blade twist, rad
κc	distance between elastic axis and center of pressure in reversed flow region, m.
$\bar{\lambda}$	inflow ratio (see Eq. (A6))
μ	tip-speed ratio
η	ratio of torsional rotations to bending displacements in the vibration mode corresponding to the lowest frequency, rad/m

4

ρ mass density of air, kg/m^3

ψ azimuth angle, rad

ω coupled frequency of the blade, rad/sec.

Ω angular velocity of a rotating blade, rad/sec.

Subscripts

A   aerodynamic

s   structural

Superscripts

B   bending

t   transpose

T   torsion

AERODYNAMICS OF ROTOR BLADES IN FORWARD FLIGHT

Background

The effects of torsional oscillations of blades become an important consideration in predicting dynamic response characteristics of high performance rotorcraft. Torsional oscillations of rotor blades have been considered by researchers in connection with stability and stall problems. The stability of coupled bending and torsional vibratory motion of rotor blades at high forward speeds has been treated by several investigators [3,4,5]. The torsional loads used in such analyses have been calculated at lower tip-speed ratios, when the coupled torsional rotations are relatively small. Under these conditions and when the blade has a sufficiently high torsional stiffness compared to the bending stiffness, the torsional motion has a minor effect on blade stability. Large torsional rotations change the aerodynamic characteristics considerably and affect the stability of the rotor blade.

The stall characteristics of rotor blades have also been studied [6,7, 8]. Ham [7,8] for instance, has shown that for stall conditions the aerodynamic damping of torsional oscillations becomes negative as the pitch angle increases. To balance such a negative aerodynamic damping, he suggested measures for addition of a positive mechanical damping.

Various investigators have been involved in determining bending and torsional aerodynamic loads on vibrating blades in forward flight [9,10]. A complete investigation of the response of rotor blades at high forward speeds requires a three-dimensional aeroelastic representation of the problem. The aerodynamics of a three-dimensional flow around the rotor blade at high forward speeds is not sufficiently developed for an accurate determination of coupled aerodynamic loads.

In the conducted investigation, effects of torsional oscillations were evaluated by quantitative comparisons of a series of structural and aerodynamic parameters. The aerodynamic loading in forward flight was determined according to the classical rotor blade analysis [3,4,11,12,13] as described in the Appendix.

Method of Solution

The equations of motion of a rotor blade can be expressed in a general matrix form as follows:

$$\underline{M}\,\ddot{\underline{r}} + \underline{D}\,\dot{\underline{r}} + \underline{K}\,\underline{r} = \underline{F}\,(t) \qquad (1)$$

where the mass, damping, and stiffness matrices can be considered as consisting of two components, structural and aerodynamic.

6

$$\underline{M} = \underline{M}_S + \underline{M}_A(\psi) \tag{2}$$

$$\underline{K} = \underline{K}_S + \underline{K}_A(\psi) \tag{3}$$

$$\underline{D} = \underline{D}_S + \underline{D}_A(\psi) \tag{4}$$

The aerodynamic terms in Eqs. (2), (3) and (4) are functions of blade azimuth position and flight conditions. Considering only the structural components of the matrices in Eqs. (2), (3), and (4) and generating a structural damping matrix proportional to the critical damping, one can obtain the eigenvectors for the following system:

$$- \omega^2 \underline{M}_S \underline{p}_i + \underline{K}_S \underline{p}_i = 0 \quad \text{where} \quad \underline{r} = Z_i \underline{p}_i \tag{5}$$

so that the generalized structural mass, stiffness, and damping terms can be calculated as

$$\alpha_i = \underline{p}_i^t \, \underline{M}_S \, \underline{p}_i \tag{6}$$

$$\beta_i = \underline{p}_i^t \, \underline{D}_S \, \underline{p}_i \tag{7}$$

$$\gamma_i = \underline{p}_i^t \, \underline{K}_S \, \underline{p}_i \tag{8}$$

and

$$\underline{p}_i^t \, \underline{M}_S \, \underline{p}_j = \underline{p}_i^t \, \underline{D}_S \, \underline{p}_j = \underline{p}_i^t \, \underline{K}_S \, \underline{p}_j = 0 \quad \text{for} \quad i \neq j \tag{9}$$

The generalized aerodynamic mass, damping, and stiffness terms are defined as

$$a_{ij}(\psi) = \underline{p}_i^t \, \underline{M}_A \, \underline{p}_j \tag{10}$$

$$b_{ij}(\psi) = \underline{p}_i^t \, \underline{D}_A \, \underline{p}_j \tag{11}$$

$$c_{ij}(\psi) = \underline{p}_i^t \, \underline{K}_A \, \underline{p}_j \tag{12}$$

Then one can write the generalized equations of motion as

$$\left\{ \alpha_i + a_{ij}(\psi) \right\} \ddot{X}_i + \left\{ \beta_i + b_{ij}(\psi) \right\} \dot{X}_i + \left\{ \gamma_i + c_{ij}(\psi) \right\} X_i = f_i(t) \tag{13}$$

In Eq. (13), the aerodynamic terms are coupled in each mode. The response problem can be analyzed from the solution of the system of second order differential equations with periodic coefficients in Eq. (13). These coefficients consist of a constant uncoupled term and a periodic coupled term.

The aerodynamic coefficients in Eq. (13) were determined for the flow regions shown in figure 1 in terms of the coupled vibration modes as described in the Appendix. These coefficients were calculated for typical flight conditions.

Analysis of the Aerodynamic Loading in Bending and Torsion

A sample blade (CH-34) was chosen to demonstrate the variation of the aerodynamic coefficients for different modes. The structural generalized mass and stiffness terms for each mode and coupling between modes were calculated as shown in table 1. The structural coupling between the lowest three modes is summarized in table 2. To illustrate the aerodynamic coupling between each of these modes, the aerodynamic stiffness and damping coefficients for the different modes were calculated as shown in figures 2, 3, and 4. From the curves one may observe the degree of coupling between the aerodynamic forces in each mode.

Each of the terms defined in Eqs. (A19), (A20), and (A21), was plotted for various tip-speed ratios for the mode corresponding to the lowest bending frequency. The aerodynamic bending stiffness, Q_{11}, represents the resultant force in the first structural mode due to unit displacement in the same mode and is plotted in figure 5. For a tip-speed ratio corresponding to the indicated operational speed of a CH-34 blade ($\mu = 0.22$), the aerodynamic bending stiffness of the blade is in the range of the calculated structural stiffness. For this case the effect of the reverse flow region is negligible. In general, as the tip-speed ratio increases, the bending stiffness values show a greater variation with changes in azimuth positions; this variation of the stiffness is greater in the forward flow region and smaller in the reverse flow region. Therefore, for high tip-speed ratios of the blade, stability problems may arise in the flapping mode due to the resulting negative bending stiffness.

As shown in figure 6, the generalized aerodynamic damping in the first bending mode, P_{11}, also depends on the tip-speed ratio of the blade. For the operating speed of the CH-34 blade, the aerodynamic damping coefficient P_{11} is found to have nearly a constant value; however, it varies considerably when the tip-speed ratio is increased. The aerodynamic damping increases in the forward flow region but it nearly vanishes for the reverse flow region. The decrease in the aerodynamic damping may be one of the reasons for the existence of increased bending amplitudes in the reverse flow region. It should be noted also that the calculated values of aerodynamic damping are found to be considerably high compared to the structural damping of the CH-34 blade. Such results suggest that a further

examination of values of characteristic aerodynamic damping for rotor blades at high forward speeds is desirable.

The aerodynamic stiffness term from the coupling of the first bending and torsional modes was also found to be dependent on the forward speed. As shown in figure 7, this stiffness term has a different sign for different flow regions at high tip-speed ratios, but it is nearly constant for low tip-speed ratios.

The variation of torsional stiffness and damping parameters with azimuth positions and tip-speed ratios is shown in figures 8, 9, 10, and 11. Aerodynamic torsional stiffness in the first mode exists only in the reverse flow region. As can be seen from figure 8, this stiffness acts as a negative feathering spring for the reverse flow region and its magnitude is proportional to the increase in tip-speed ratios. Accordingly, the total torsional stiffness of the blade has lower values in the reverse flow region. The structural torsional stiffness of the blade must be increased in order to overcome this negative aerodynamic stiffness.

The variation of the torsional damping for various tip-speed ratios was also investigated and is shown in figure 9. For high tip-speed ratios, torsional damping becomes higher for the forward flow region, while for the reverse flow region the aerodynamic torsional damping vanishes. The variations of the coupled aerodynamic stiffness and damping terms are shown in figures 10 and 11. These coupled terms also exist only for the reverse flow region and increase proportionally to the tip-speed ratios.

ANALYSIS OF THE COUPLED EQUATIONS OF MOTION
OF A ROTOR BLADE IN FORWARD FLIGHT

Method of Solution

The coupled equations of motion of rotor blades in bending and torsion can be expressed in terms of the generalized mass, damping and stiffness coefficients. These equations are:

$$\alpha_i^B \ddot{X}_i + \left[\beta_i^B + P_{ij}(\psi) \right] \dot{X}_{i,j} + \left[\gamma_i^B + Q_{ij}(\psi) \right] X_{i,j} + Y_h \, m_{ih}(\psi) = L_{ei}(\psi)$$

(14)

for the bending motion, and

$$\alpha_i^T \ddot{Y}_i + \left[\beta_i^T + p_{ij}(\psi) \right] \dot{Y}_{i,j} + \left[\gamma_i^T + q_{ij}(\psi) \right] Y_{i,j} + R_{ih}(\psi) X_h$$

$$+ S_{ih}(\psi) \dot{X}_h = M_{ei}(\psi) \qquad (15)$$

for the torsional motion where (X_i, Y_i) is the coupled structural mode.

Eqs. (14) and (15) can be treated as a system of differential equations with periodic coefficients to analyze the dynamic response of rotor blades at high forward speeds. An approximation of the response of the coupled system can be examined from the analysis of a two-degree-of-freedom system.

The displacements and rotations of the blade can now be assumed as follows:

$$X_1 = X_o e^{\omega t} \qquad (16)$$

and

$$Y_1 = Y_o e^{\omega t} = \eta X_o e^{\omega t} \qquad (17)$$

where η is the ratio of torsional rotations to bending displacements. Eqs. (14) and (15) can be written for the free vibrations as follows:

$$\omega^2 \alpha_1^B + \left[\beta_1^B + P_{11}(\psi) \right] \omega + \left[\gamma_1^B + Q_{11}(\psi) \right] + \eta m_{11}(\psi) = 0 \qquad (18)$$

$$\eta \left\{ \omega^2 \alpha_1^T + \left[\beta_1^T + p_{11}(\psi) \right] \omega + \left[\gamma_1^T + q_{11}(\psi) \right] \right\} + R_{11}(\psi) + S_{11}(\psi) \omega = 0 \qquad (19)$$

These two algebraic equations can be solved to obtain the following expressions:

$$\eta = - \frac{R_{11}(\psi) + \omega S_{11}(\psi)}{\omega^2 \alpha_1^T + \left[\beta_1^T + p_{11}(\psi) \right] \omega + \gamma_1^T + q_{11}(\psi)} \qquad (20)$$

and

$$\left\{ \omega^2 \alpha_1^B + \left[\beta_1^B + P_{11}(\psi) \right] \omega + \gamma_1^B + Q_{11}(\psi) \right\} \quad \left\{ \omega^2 \alpha_1^T + \left[\beta_1^T + p_{11}(\psi) \right] \omega \right.$$

$$\left. + \gamma_1^T + q_{11}(\psi) \right\} = m_{11}(\psi) \left[R_{11}(\psi) + \omega \, S_{11}(\psi) \right] \qquad (21)$$

Eq. (21) is a fourth order polynomial which can be solved to obtain the corresponding lowest frequencies of the coupled equations of motion. From Eq. (20) the degree of coupling can be calculated. One has to consider the variation of each one of the coefficients of Eqs. (20) and (21) in order to explain the obtained results. According to the azimuth position of the blade, the coefficients of Eqs. (20) and (21) exhibit different characteristics.

In forward flow region - For zero aerodynamic damping ($\kappa = 0.5$) in the forward flow region, the coupled damping and stiffness terms (R_{11} and S_{11}) vanish as shown in figures 9 and 10. Then, Eqs. (18) and (19) become uncoupled, as can be seen from Eq. (21). The torsional oscillations can be determined for this case only from the structural and aerodynamic properties of the blade in torsion. However, for an eccentricity between elastic and aerodynamic axes, ($\kappa \neq 0.5$), a complete solution of Eq. (21) is necessary.

In reverse flow region - When the blade enters the reverse flow region, the magnitudes of the coupled terms are considerably higher. The coupled motion of the blade can then be analyzed from the complete solution of Eq. (21). The coupled frequencies are strongly dependent on the degree of coupling in this region.

The magnitudes of the torsional oscillations can be analyzed in terms of the following two factors:

a)   the ratio of torsional to bending frequency (ω_T^2/ω_B^2)

b)   the degree of coupling between torsional and bending modes.

If the magnitudes of the torsional and bending frequencies are close, a major portion of the torsional oscillations occur in the mode corresponding to the torsional frequency. As can be seen from figures 7 and 8, the value of the torsional frequency ω_T depends on the negative aerodynamic stiffness and the decrease in the aerodynamic damping for the reverse flow region. When the torsional frequency is much higher than the bending frequency and the coupling between bending and torsional modes is significant, the torsional oscillations are mostly in the coupled mode corresponding to the lowest bending frequency. The presence of torsional vibrations, coupled with these bending oscillations, is indicated from the results of the harmonic analysis and from experimental measurements of pitching and

11

plunging motion of rotor blades [8].

Sensitivity Analysis of Torsional Vibration Characteristics
of a Sample Blade

The sensitivity analysis of coupled torsional and bending vibrations was carried out for a sample blade (CH-34) as described above. Quantitative results were obtained from the solution of Eqs. (20) and (21) for different flight conditions and varying the blade properties.

Figures 12-14 show the response of the blade in forward flight for coinciding elastic and aerodynamic axes. For the operational speed of the sample blade (μ = 0.22), the aerodynamic damping and the natural bending frequency show a periodic variation, corresponding to the variation of bending stiffness and damping coefficients in figures 2 and 3. As shown in figure 9, torsional damping varies also periodically with changing azimuth positions. However, the constant torsional structural stiffness is the important factor in determining torsional frequency, as can be seen from figure 8. The coupling ratio between torsional and bending modes (η) exists only in the reverse flow region and reaches a maximum at an azimuth position of 270°.

A detailed torsional sensitivity analysis of the rotor blade was further developed starting from the ideal uncoupled case. The first term to be included in the sensitivity analysis was the effect of the eccentricity between elastic and mass axes. The effects of structural coupling on blade response, considering only the structural terms, were discussed in the first report [1]. The analysis can be extended to include the additional aerodynamic uncoupled loading of the blade. As shown in figures 15-17, in this case, bending and torsional frequencies were insensitive to the addition of structural eccentricity of the blade. Such behavior can be explained in terms of the relative magnitudes of structural and aerodynamic coefficients. As described in the first report, bending frequencies are not sensitive to the structural eccentricity (x_θ) even without considering the aerodynamic

loading. The importance of this effect is indicated in the variation of coupling ratio with varying eccentricities. The coupling in the bending mode is increased uniformly for all positions of the blade for an eccentricity of x_θ = -1, and it exists mostly in the forward region for x_θ = 1. The coupling ratio for the torsional mode is increased with additional eccentricity. The torsional frequencies are also increased as shown in figure 15.

The second term considered in the torsional sensitivity analysis of the blade was the effect of the relative position of aerodynamic axis with respect to the elastic axis. The exact position of the aerodynamic axis varies with time as the azimuth position of the blade changes in forward flight. The results obtained from the sensitivity analysis can be used in this case to evaluate the effects of the changes in the aerodynamic and elastic axes, both qualitatively and quantitatively. The previous results were obtained

for an ideal case, when the blade oscillates around the one-quarter chord-width and the distance between the elastic and aerodynamic axes is one-half chord-width for both reverse and forward flows ($\kappa = 0.5$). To investigate the effect of the changes in the relative positions of the aerodynamic and elastic axes, the aerodynamic axis was moved in a symmetric fashion for forward and reverse flow by changing κ to 0.4 and 0.6 respectively. The additional aerodynamic pitching moments were included in the expressions in the Appendix for varying positions of elastic and aerodynamic axes. The obtained results were illustrated in figures 18-21.

Two cases ($\kappa = 0.6$, $\kappa = 0.4$) describe the behavior when the aerodynamic axis is fore and aft of the elastic axis. The bending frequencies of the rotor blade are reduced considerably for the entire rotor disc when $\kappa = 0.6$. However, for $\kappa = 0.4$ these frequencies show a consistent variation for different azimuth positions. Compared to the case $\kappa = 0.5$, the response of the blade is stabilized for azimuth positions $90° < \psi < 270°$ for $\kappa = 0.4$. This improvement is due to the additional stiffness obtained from the coupling with the torsional mode. On the other hand, the coupling ratio has been increased considerably compared to the uncoupled case ($\kappa = 0.5$). For $\kappa = 0.4$, the blade also exhibits an underdamped behavior for azimuth positions $90° < \psi < 360°$.

The variation of torsional frequencies with coupling between mass and elastic axes is also an important consideration in the response analysis. While torsional frequencies are increased for $\kappa = 0.4$, the blade is unstable in a basically torsional mode for $\kappa = 0.6$. These results indicate that the blade vibrations may become unstable in a predominantly torsional mode, when the aerodynamic axis moves ahead of the elastic axis. The torsional vibrations are overdamped for $\kappa = 0.4$.

From the above results, the sensitivity of torsional characteristics of the CH-34 blade was described for the blade operating speed ($\mu = 0.22$). Another important element of the investigation of torsional sensitivity characteristics of rotor blades is the changing flight conditions. The torsional and bending vibration frequencies and the coupling between the modes were calculated for different flight conditions and different positions of the aerodynamic and elastic axes. Figures 22-27 indicate the changes in the bending frequencies and coupling ratios with increasing forward speeds.

As the tip-speed ratio increases, the bending frequencies show a periodic variation with changing azimuth positions and the values of the frequencies are highest at the forward flow region. These results can be interpreted again in terms of the values of bending stiffness in figure 2. The bending vibrations become unstable for azimuth position $90° < \psi < 180°$. The frequencies in the reverse flow region remain relatively low. For $\kappa = 0.5$ the coupling ratio exists again only for the reverse flow region. Another possibility of instability for $270° < \psi < 360°$ exists in the reverse flow region due to the low torsional frequencies in this region.

For $\kappa = 0.4$ the effect of tip-speed ratios is considerably smaller in

the bending modes due to the aerodynamic coupling terms in bending and tor-
sion. In this case coupling improves the blade response by removing the in-
stability region. In the reverse flow region the frequencies show a more
rapid change as compared to $\kappa = 0.5$.

For $\kappa = 0.6$ the blade becomes unstable in a mainly torsional mode. The
bending frequencies vary rather strongly as the tip-speed ratios increase,
due to the coupling with the unstable torsional motion. The ratio of cou-
pling shows a similar unstable behavior.

Variations of torsional frequencies and coupling ratios of rotor blades
for different forward flight conditions are illustrated in figures 28-33.
In the reverse flow region, the torsional frequencies change considerably
with increasing tip-speed ratios. The instability in the reverse flow re-
gion can be explained in terms of the negative stiffness coefficient in fig-
ure 8. The coupling ratio for the torsional displacement indicates an un-
derdamped behavior and varies slightly with increasing tip-speed ratios.
Torsional frequencies are found to be sensitive to tip-speed ratios, also
for $\kappa = 0.4$. The coupling increases the torsional frequencies in the re-
verse flow region compared to the uncoupled case $\kappa = 0.5$. The coupling ra-
tio for this case indicates an underdamped behavior for high tip-speed ra-
tios.

For $\kappa = 0.6$ the effect of tip-speed ratios was also tested. The tor-
sional frequencies decrease proportionally to the increase in the tip-speed
ratios. The ratio of coupling for this case indicates an underdamped behav-
ior and shows a change in the sign of the coupling ratio in forward and re-
verse flow regions.

After discussing the effects of structural and aerodynamic coupling
separately, a combination of eccentricities between elastic, mass and aero-
dynamic axes is presented as shown in figures 34 and 35. In this case, for
$\kappa = 0.4$, $\mu = 0.22$, the structural eccentricity x_θ was varied for $x_\theta = -1, 0,$
1. As can be seen from figure 34, the bending and torsional frequencies
were affected only slightly with this structural eccentricity. Such behav-
ior can be explained in terms of the sensitivity of rotor blades to struc-
tural eccentricities, as described in the first report, and the relative
magnitudes of structural and aerodynamic loads, as discussed in this report.

Conclusions

The presented investigation of coupled bending and torsional vibration
characteristics of rotor blades has shown the effectiveness of sensitivity
analysis for studying dynamic response problems. The importance of the tor-
sional degrees-of-freedom was established in terms of structural and aerody-
namic components of the aeroelastic analysis of rotor blades.

The sample blade analysis has shown that the aerodynamic and structural
coupling terms in the equations of motion have to be considered to obtain

14

realistic results for vibration frequencies and mode shapes. From the developed sensitivity analysis of the mathematical model the significance of blade design parameters can be determined and used to improve the blade response and stability. The investigation has also shown the importance of the aerodynamic terms in the vibration analysis of blades in forward and reverse flow regions at high tip-speed ratios.

APPENDIX

CALCULATION OF THE AERODYNAMIC LOADING IN FORWARD FLIGHT

The airflow over the entire rotor disk, at any azimuth position, was analyzed in the three regions shown in figure 1 [13]. In region (1) the blade encounters only forward flow; in region (3) only reversed flow. In the mixed flow region (2), blade elements for radial positions from $r/R = 0$ to $r/R = -\mu \sin \psi$ operate in the reverse flow and those from $r/R = -\mu \sin \psi$ to $r/R = 1$ operate in normal flow. The angle defining azimuth positions in region (2) is defined as

$$\varepsilon = \begin{cases} \text{Arc sin } \dfrac{B}{\mu} & B \leq \mu \\[3mm] \dfrac{\pi}{2} & B > \mu \end{cases} \tag{A1}$$

Blade Flapping Motion: - From the two-dimensional theory the lift co-efficient of a blade element is assumed to be [14]

$$C_L = a\, \alpha_r \tag{A2}$$

where α_r is the angle of attack given by

$$\alpha_r = \frac{U_p}{U_t} + \theta_p + \theta \tag{A3}$$

U_t and U_p are the tangential and normal components of the resultant air velocity respectively, and they can be written as

$$U_t = \Omega R + \mu \Omega R \sin \psi \tag{A4}$$

$$U_p = \overline{\lambda}\Omega R + \frac{dh}{dt} - \mu \Omega R \beta \cos \psi \tag{A5}$$

where

$$\overline{\lambda} = \frac{V \sin \alpha_r - v_i}{\Omega R} \tag{A6}$$

and

$$\mu = \frac{V}{\Omega R} \tag{A7}$$

16

The pitch angle of the blade section is defined by

$$\theta_T = \theta_p + \theta = \theta_o + \theta_s \sin \psi + \theta_c \cos \psi + \frac{r}{R} \theta_1 + \theta \qquad (A8)$$

where θ_p represents the angle of pitch control and θ is the pitch angle due to torsion.

The torsional rotation θ, the bending displacement h and rotation β can be defined in terms of the uncoupled structural modes of a rotating blade as follows:

$$\theta = Y_i \overline{\theta}_i \qquad (A9)$$

$$h = X_i \overline{h}_i \qquad (A10)$$

$$\beta = X_i \overline{\beta}_i \qquad (A11)$$

where $\overline{\theta}_i$, $\overline{h}_i$, and $\overline{\beta}_i$ are the eigenfunctions obtained from Eq. (5). For two-dimensional flow the lift on the blade element can be written as

$$dL = \frac{1}{2} \rho V^2 C_L c \, dr \qquad (A12)$$

where V is the resultant velocity at the blade element. Since it is assumed that U_p/U_t is small,

$$V = U_t \qquad (A13)$$

The generalized forces in bending can be written, using the principle of virtual work, as

$$\int_r h \, dL = \int_0^R \frac{1}{2} \rho V^2 C_L c h \, dr \qquad (A14)$$

or

$$\int_r \overline{h}_i \, dL = \int_0^R \frac{1}{2} \rho V^2 C_L c \overline{h}_i \, dr \qquad (A15)$$

Substituting Eqs. (A2) and (A13) into Eq. (A15), the generalized lift force in each mode can be written as

$$\int_r h_i \, dL = \frac{1}{2} \rho ac \int_0^R U_t^2 \overline{h}_i \left(\frac{U_p}{U_t} + \theta_p + \theta \right) dr$$

$$= \frac{1}{2} \rho ac \int_0^R U_t \overline{h}_i \left(\overline{\lambda} \Omega R + \frac{dh}{dt} - \mu \Omega R \beta \cos \psi \right) dr \qquad (A16)$$

$$+ \frac{1}{2} \rho ac \int_0^R U_t^2 \overline{h}_i \left(\left[\theta_o + \theta_s \sin \psi + \theta_c \cos \psi + \frac{r}{R} \theta_1 \right] + \theta \right) dr$$

This equation can now be simplified to

$$\int_r \overline{h}_i \, dL = F_i (\psi) + Y_h m_{ih} (\psi) + X_j Q_{ij} (\psi) + \dot{X}_j P_{ij} (\psi) \qquad (A17)$$

The generalized force is

$$F_i (\psi) = \frac{1}{2} \rho ac \int_0^R U_t \overline{h}_i \left[\overline{\lambda} \Omega R + U_t \left(\theta_o + \theta_s \sin \psi + \theta_c \cos \psi + \frac{r}{R} \theta_1 \right) \right] dr$$

$$\qquad (A18)$$

The generalized coupled torsional stiffness is

$$m_{ih} (\psi) = \frac{1}{2} \rho ac \int_0^R U_t^2 \overline{h}_i \theta_h \, dr \qquad (A19)$$

The generalized bending stiffness is

$$Q_{ij} (\psi) = - \frac{1}{2} \rho ac \int_0^R U_t \overline{h}_i \mu \Omega R \overline{\beta}_j \cos \psi \, dr \qquad (A20)$$

The generalized bending damping is

$$P_{ij} (\psi) = \frac{1}{2} \rho ac \int_0^R U_t \overline{h}_i \overline{h}_j \, dr \qquad (A21)$$

Blade Torsional Motion: - Considering only two kinds of aerodynamic feathering moments, M_{F1} and M_{F2}, for a two-dimensional airfoil [4], the torsional equations of motion were written as follows:

a) The first feathering moment, M_{F1}, will occur due to the steady aerodynamic lift and the position of the aerodynamic center in forward and reverse flow regions. The lift generated by the reversed flow can be written as

$$dL_R = -\frac{1}{2} ca'\rho \, U_t^2 \, \alpha_r \, dr \tag{A22}$$

The first feathering moment can then be written as

$$dM_{F1} = \frac{1}{2} c^2 \kappa a'\rho \, U_t^2 \, \alpha_r \, dr \tag{A23}$$

Using the principle of virtual work, the generalized moments at each mode can be written as

$$\int_r \overline{\theta}_i \, dM_{F1} = \int_0^R \frac{1}{2} c^2 \kappa a'\rho \, U_t^2 \, \overline{\theta}_i \left(\frac{U_p}{U_t} + \theta_p + \theta \right) dr$$

$$= \frac{1}{2} c^2 \kappa a'\rho \int_0^R \left\{ \overline{\theta}_i \, U_t \left[\overline{\lambda} \, \Omega R + \frac{dh}{dt} - \mu\Omega R\beta \cos\psi \right] \right. \tag{A24}$$

$$\left. + \overline{\theta}_i \, U_t^2 \left[\theta_p + \theta \right] \right\} dr$$

Eq. (A24) can be simplified as

$$\int_r \overline{\theta}_i \, dM_{F1} = G_i(\psi) + X_k R_{ki}(\psi) + \dot{X}_k S_{ki}(\psi) + Y_j q_{ij}(\psi) \tag{A25}$$

b) For the second feathering moment, M_{F2}, only one unsteady aerodynamic effect is considered and that is the moment due to forces caused by the damping of the pitching motion. Assuming that the feathering motion occurs about the 1/4 chord-width, the lift due to blade pitching velocity has two components: one at 1/4 chord-width and one at 3/4 chord-width. The lift force can be expressed as

19

$$dL = \frac{1}{8} c^2 a\rho \, U_t \, \dot{\alpha}_r \, dr \qquad (A26)$$

where

$$\dot{\alpha}_r = \dot{\theta}_p + \dot{\theta} \qquad (A27)$$

The lift force in Eq. (A26) generates a feathering moment

$$dM_{F2} = -\frac{1}{16} c^3 a\rho \, U_t \, \dot{\alpha}_r \, dr \qquad (A28)$$

which is valid for the forward flow. Using the principle of virtual work, the generalized moments for this case can be written as

$$\int_r \overline{\theta}_i \, dM_{F2} = - \int_0^R \frac{1}{16} c^3 a\rho \, U_t \, \overline{\theta}_i \, \dot{\alpha}_r \, dr$$

$$= -\frac{1}{16} c^3 a\rho \int_0^R \left[\dot{Y}_j \, U_t \, \overline{\theta}_i \, \overline{\theta}_j + U_t \, \overline{\theta}_i \, \dot{\theta}_p \right] dr \qquad (A29)$$

$$= \dot{Y}_j \, p_{ij} + C_{\theta i} \, \dot{\theta}_p$$

Combining Eqs. (A25) and (A29), the generalized torsional moment equation can be written as

$$\int_r \overline{\theta}_i \, dM_F = \dot{Y}_j \, p_{ij}(\psi) + C_{\theta i}(\psi) \, \dot{\theta}_p + G_i(\psi) + X_k \, R_{ki}(\psi) + \dot{X}_k \, S_{ki}(\psi)$$

$$+ Y_j \, q_{ij}(\psi) \qquad (A30)$$

where the generalized torsional damping is

$$p_{ij}(\psi) = - \int_0^R \frac{1}{16} c^3 a\rho \, U_t \, \overline{\theta}_i \, \overline{\theta}_j \, dr \qquad (A31)$$

The generalized torsional stiffness is

$$q_{ij}(\psi) = \int_0^R \frac{1}{2} c^2 \kappa a' \rho U_t^2 \bar{\theta}_i \bar{\theta}_j \, dr \qquad \text{(A32)}$$

The generalized coupled bending stiffness is

$$R_{ki}(\psi) = - \int_0^R \frac{1}{2} c^2 \kappa a' \rho \mu \Omega R \bar{\beta}_k U_t \bar{\theta}_i \cos \psi \, dr \qquad \text{(A33)}$$

The generalized coupled bending damping is

$$S_{ki}(\psi) = \int_0^R \frac{1}{2} c^2 \kappa a' \rho \bar{h}_k U_t \bar{\theta}_i \, dr \qquad \text{(A34)}$$

The generalized control moment damping is

$$C_{\theta i}(\psi) = - \int_0^R \frac{1}{16} c^3 a \rho U_t \bar{\theta}_i \, dr \qquad \text{(A35)}$$

The generalized control moment is

$$G_i(\psi) = \int_0^R \frac{1}{2} c^2 \kappa a' \rho U_t \bar{\theta}_i \left(U_t \theta_p + \bar{\lambda} \Omega R \right) \, dr \qquad \text{(A36)}$$

REFERENCES

1. Bratanow, T., and Ecer, A.: Sensitivity Analysis of Torsional Vibration Characteristics of Helicopter Rotor Blades, Part I, Aerodynamics and Sensitivity Analysis. To be published as a NASA report.

2. Miller, R.H.: Rotor Blade Harmonic Airloading. AIAA J., Vol. 2, No. 7, July, 1964, pp.1254-1269.

3. Crimi, P.: A Method for Analyzing the Aeroelastic Stability of a Helicopter Rotor in Forward Flight. NASA CR-1332, Aug., 1969.

4. Kuczynski, W.A., and Sharpe, D.L.: Hingeless Rotor Characteristics at High Advance Ratios. AIAA 4th Fluid and Plasma Dynamics Conference, Palo Alto, Calif., June 21-23, 1971.

5. Piarulli, V.J., and White, R.P. Jr.: A Method for Determining the Characteristic Functions Associated with the Aeroelastic Instabilities of Helicopter Rotors in Forward Flight. NASA CR-1577, 1970.

6. Fisher, R.K. Jr., and McCroskey, W.J.: Detailed Aerodynamic Measurements on a Model Rotor in the Blade Stall Regime. Presented at the 27th Annual National V/STOL Forum of the Am. Helicopter Soc., Washington, D.C., May, 1971.

7. Ham, N.D.: Aerodynamic Loading on a Two-Dimensional Airfoil during Dynamic Stall. AIAA J., Vol. 6, No. 10, Oct., 1968.

8. Ham, N.D., and Young, M.I.: Limit Cycle Torsional Motion of Helicopter Blades Due to Stall. J. Sound Vib., Vol. 4, No. 3, 1966, pp. 431-444.

9. Kuczynski, W.A., and Sissingh, G.J.: Research Program to Determine Rotor Response Characteristics at High Advance Ratios. NASA CR-114290, Feb., 1971.

10. Yntema, R.T.: Simplified Procedures and Charts for the Rapid Estimation of Bending Frequencies of Rotating Beams. NACA TN 3459, 1955. (Supersedes NACA RM L54G02).

11. Perisho, C.H.: Analysis of the Stability of a Flexible Rotor Blade at High Advance Ratio. J. of the Am. Helicopter Soc., Vol. 4, No. 2, April, 1959, pp. 4-18.

12. Sissingh, G.J.: Dynamics of Rotors Operating at High Advance Ratios. J. of the Am. Helicopter Soc., Vol. 13, No. 3, July, 1968, pp. 56-63.

13. Sissingh, G.J., and Kuczynski, W.A.: Investigations of the Effect of Blade Torsion on the Dynamics of the Flapping Motion. J. of the Am. Helicopter Soc., April, 1970.

14. Gessow, A., and Myers, G. Jr.: Aerodynamics of the Helicopter. Frederick Ungar Publishing Co., New York, 1952.

TABLE 1a. Generalized Structural Mass ($\alpha_{ij} = \underline{p}_i^t \underline{M} \underline{p}_j$), $x_\theta = .0254$ m. for Uncoupled Modes of CH-34 Blade

		Bending Modes			Torsional Modes		
		1	2	3	1	2	3
		Kg. sec.²/m.			Kg. sec.²		
Bending Modes	1.	3.0160	0.0000	0.0000	0.8399	$-.1784 \times 10^{-2}$	$-.2592 \times 10^{-2}$
	2.	0.0000	1.9366	0.0000	$-.3127 \times 10^{-2}$	$-.0640$	$.8074 \times 10^{-2}$
	3.	0.0000	0.0000	1.8445	$.3221 \times 10^{-2}$	$.8977 \times 10^{-2}$	.0604
		Kg. sec.²			Kg. sec.² m.		
Torsional Modes	1.	0.0839	$-.3127 \times 10^{-2}$	$.3221 \times 10^{-2}$	$.2817 \times 10^{-1}$	0.0000	0.0000
	2.	$-.1784 \times 10^{-2}$	$-.0640$	$.8977 \times 10^{-2}$	0.0000	$.2668 \times 10^{-1}$	0.0000
	3.	$-.2592 \times 10^{-2}$	$.8074 \times 10^{-1}$	.0604	0.0000	0.0000	$.2579 \times 10^{-1}$

24

TABLE 1b. Generalized Structural Stiffness $(Y_{ij} = \underline{p}_i^t \underline{K} \underline{p}_j)$, $x_\theta = .0254$ m. for Uncoupled Modes of CH-34 Blade

		Bending Modes			Torsional Modes		
		1	2	3	1	2	3
			Kg/m.			Kg.	
Bending Modes	1.	1.8058×10^3	0.0000	0.0000	$-.4378 \times 10^2$	$-.1449 \times 10^3$	$-.1407 \times 10^3$
	2.	0.0000	8.4362×10^3	0.0000	$-.2636 \times 10^1$	$.7629 \times 10^2$	$.1960 \times 10^3$
	3.	0.0000	0.0000	2.6117	$-.0763 \times 10^1$	$.3531 \times 10^1$	$-.1082 \times 10^3$
			Kg.			Kg. m.	
Torsional Modes	1.	$-.4378 \times 10^2$	$-.2636 \times 10^1$	$-.0763 \times 10^1$	8.4207×10^2	0.0000	0.0000
	2.	$-.1449 \times 10^3$	$.7629 \times 10^2$	$.3532 \times 10^1$	0.0000	7.2324×10^3	0.0000
	3.	$-.1407 \times 10^3$	$.1960 \times 10^3$	$-.1082 \times 10^3$	0.0000	0.0000	2.0219×10^4

TABLE 2. Uncoupled Generalized Structural Mass (α_i), Critical Damping (β_i), and Stiffness (γ_i) of CH-34 Blade

	Bending Modes			Torsional Modes		
	1	2	3	1	2	3
α_i	3.0160 (kg.sec.^{2}/m)	1.9306	1.8445	4.4356x10^2 (Kg.sec.^{2}/m)	4.2012x10^2	4.0622x10^2
β_i	1.4759x10^2 (Kg.sec./m.)	2.5524x10^2	4.3898x10^2	1.5339x10^4 (Kg.sec./m.)	4.3750x10^4	7.1936x10^4
γ_i	1.8058x10^1 (Kg./m)	8.4362x10^3	2.6117x10^4	1.3261x10^6 (Kg./m.)	1.1389x10^5	3.1848x10^7

normal flow

reverse flow

Ω

$\psi = \pi$

1

2 2

ϵ ϵ

3

$\psi = 0$

ψ (degrees)

Fwd
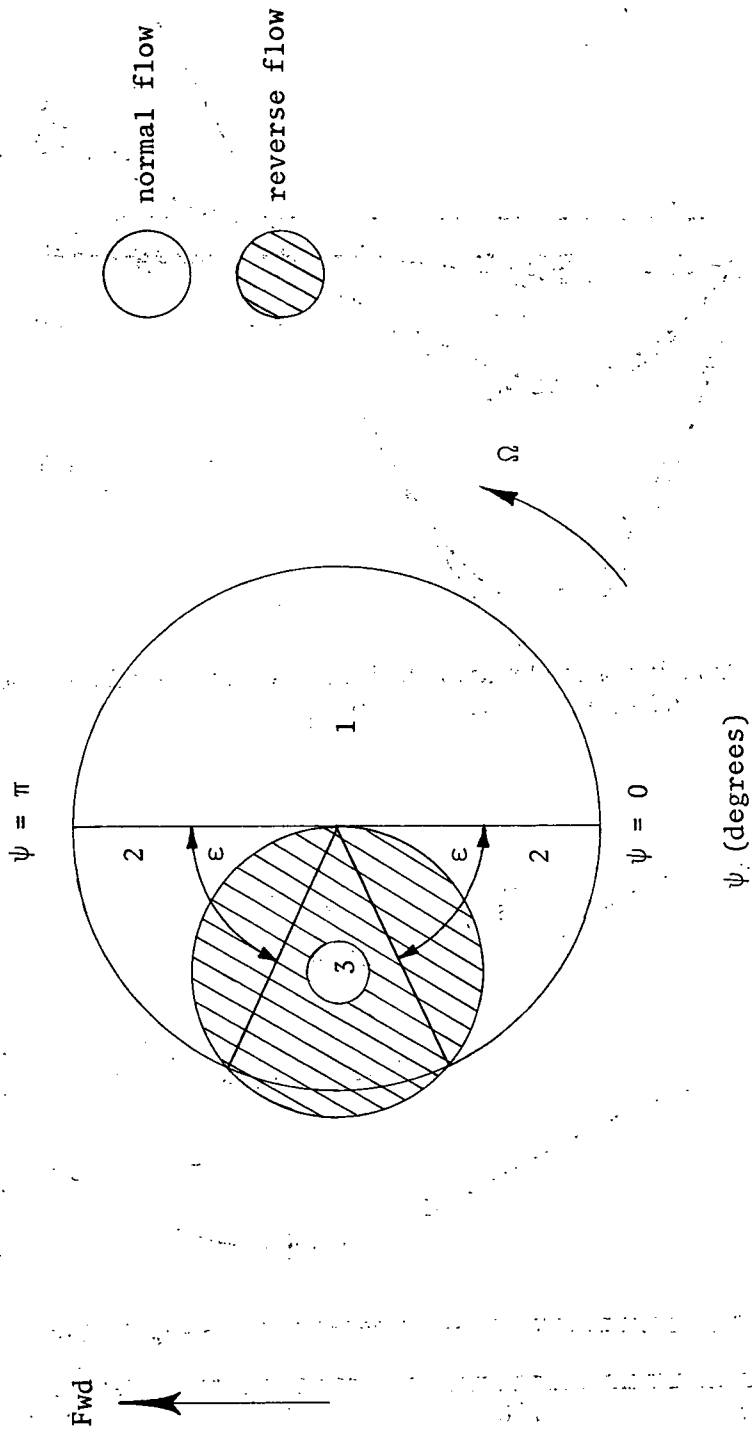
Fig. 1. The Flow Regions for Rotor Blades in Forward Flight, ($\mu = 1.2$).

27
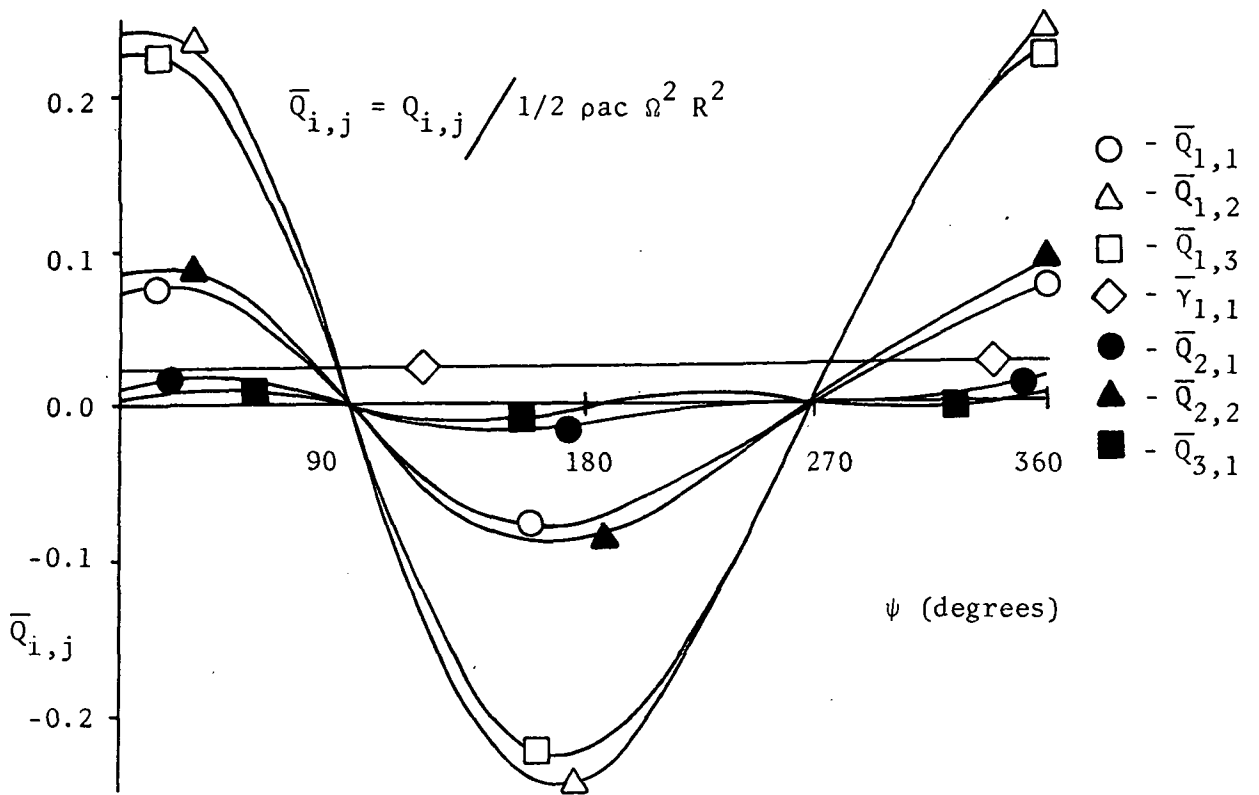
Fig. 2 Variation of Aerodynamic Bending Stiffness with Blade Azimuth
Positions, ($\mu = 0.22$, $\kappa = 0.5$, $x_\theta = 0.0$).
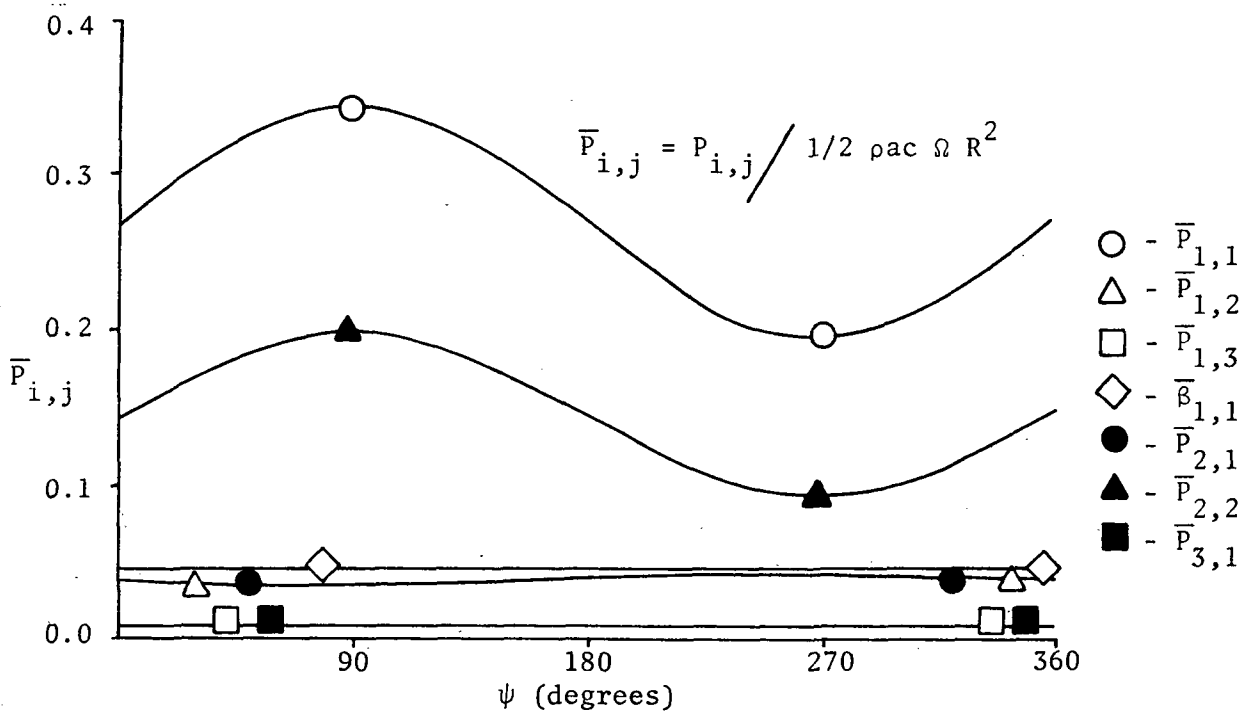
Fig. 3 Variation of Aerodynamic Bending Damping with Blade Azimuth
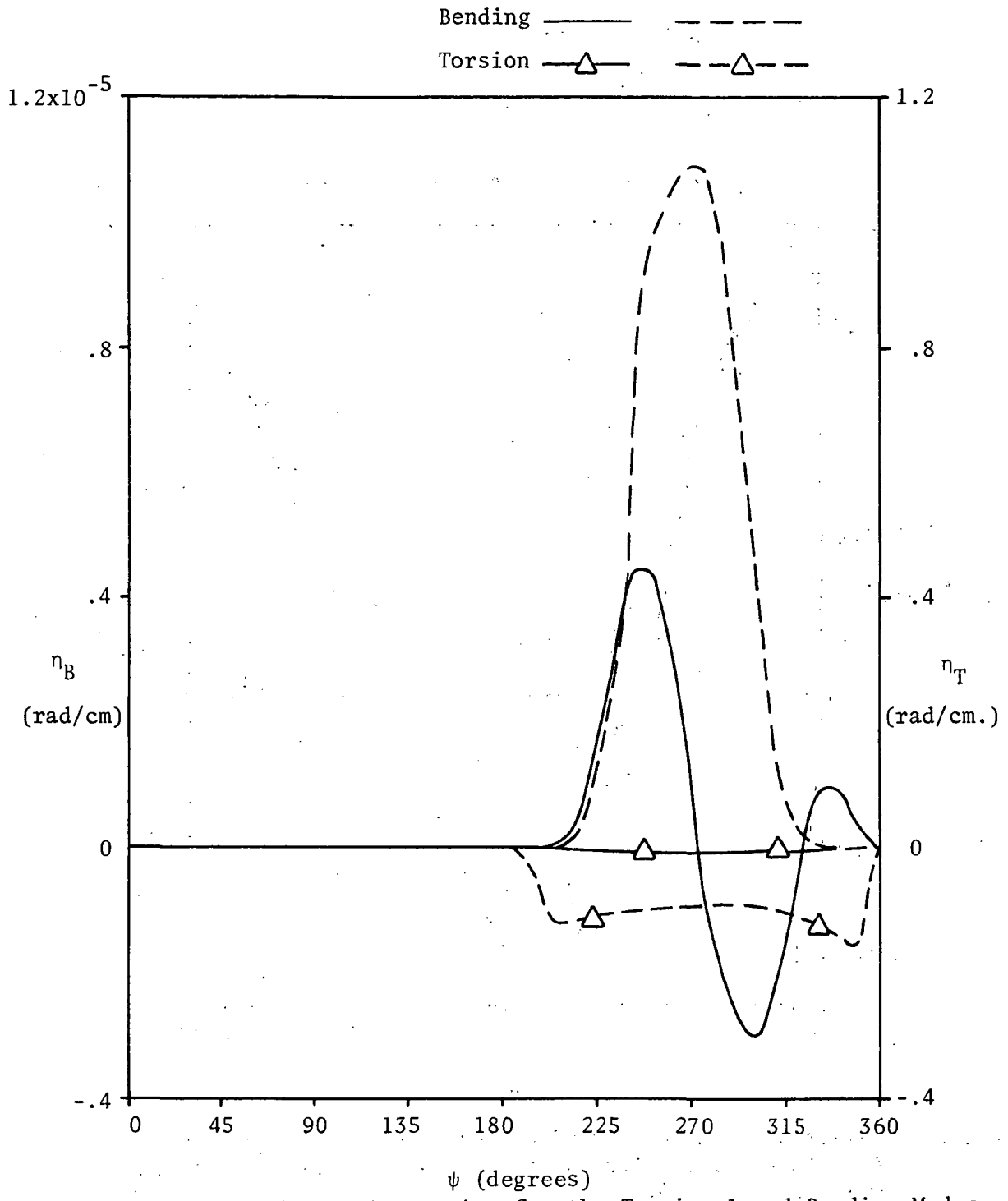Positions, ($\mu = 0.22$, $\kappa = 0.5$, $x_\theta = 0.0$).

28
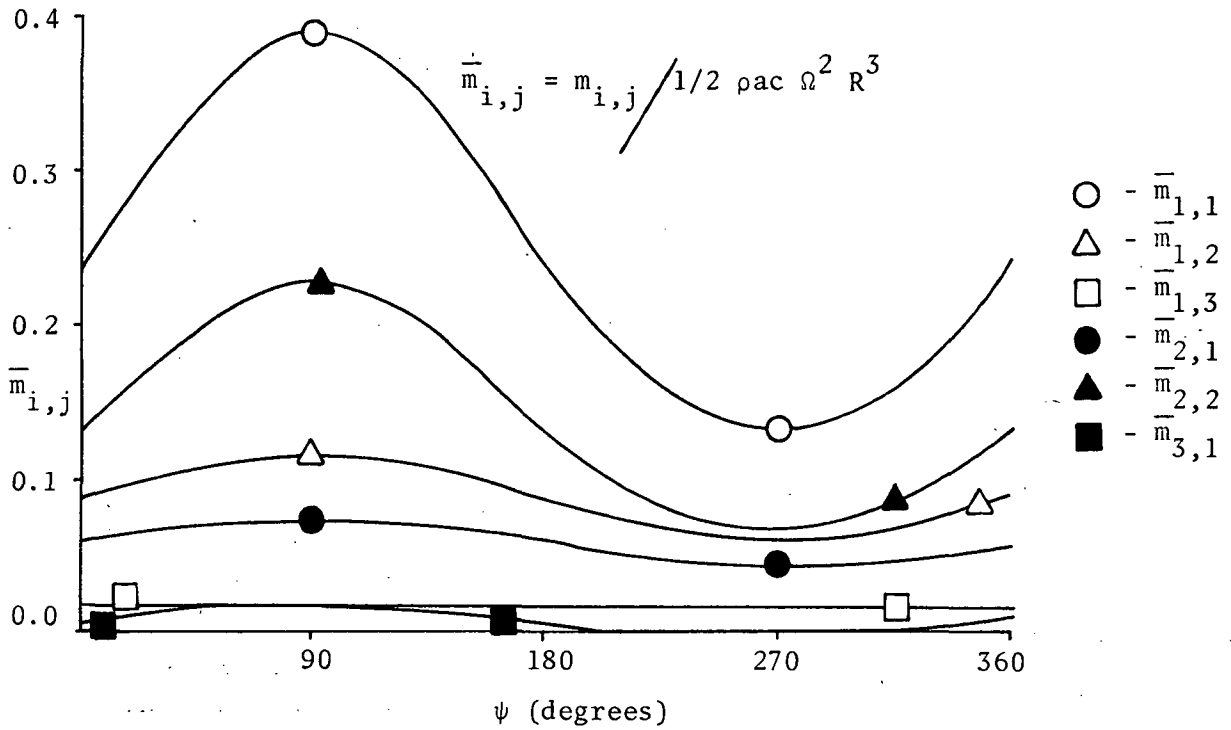
Fig. 4 Variation of Aerodynamic Bending Coupling with Blade Azimuth
Positions, (μ = 0.22, κ = 0.5, x_θ = 0.0).

$$\bar{m}_{i,j} = m_{i,j} \Big/ 1/2\ \rho ac\ \Omega^2 R^3$$

$\bigcirc$ – $\bar{m}_{1,1}$
$\triangle$ – $\bar{m}_{1,2}$
$\square$ – $\bar{m}_{1,3}$
$\bullet$ – $\bar{m}_{2,1}$
$\blacktriangle$ – $\bar{m}_{2,2}$
$\blacksquare$ – $\bar{m}_{3,1}$

$\bigcirc$ – μ = 1.8
$\triangle$ – μ = 1.0
$\square$ – μ = .22
$\diamondsuit$ – $\bar{\delta}_{1,1}$

$$\bar{Q}_{1,1} = Q_{1,1} \Big/ 1/2\ \rho ac\ \Omega^2 R^2$$
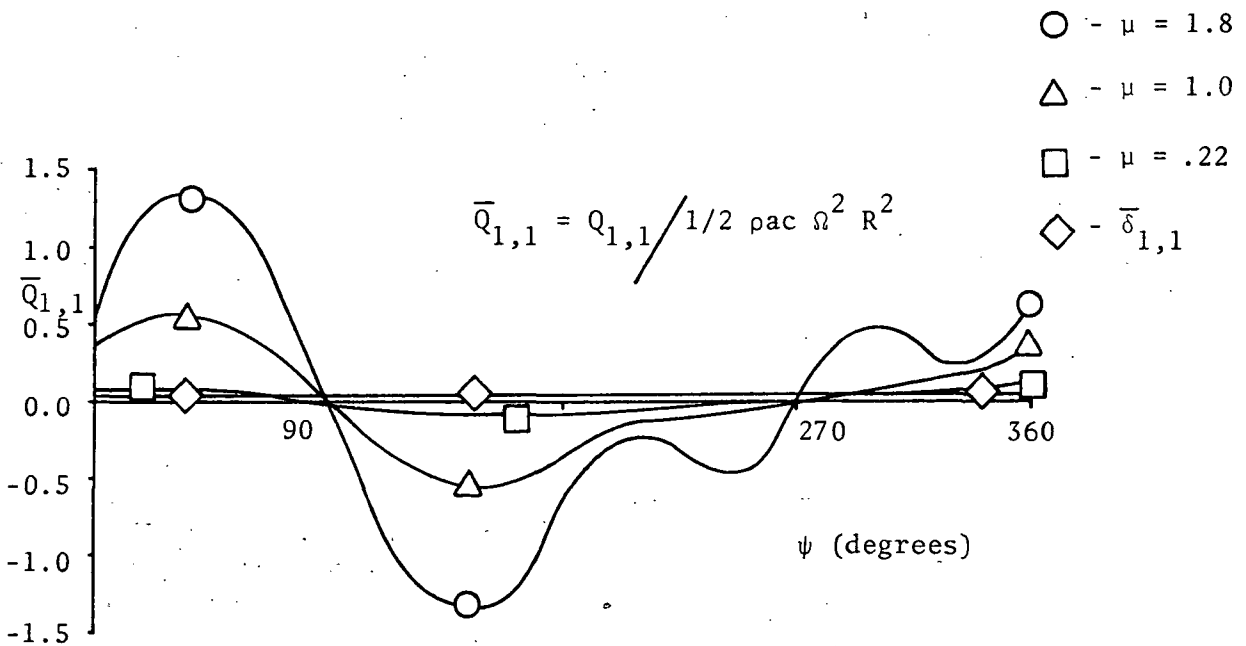
Fig. 5 Aerodynamic Stiffness in First Bending Mode at Various Advance
Ratios, (κ = 0.5, x_θ = 0.0).
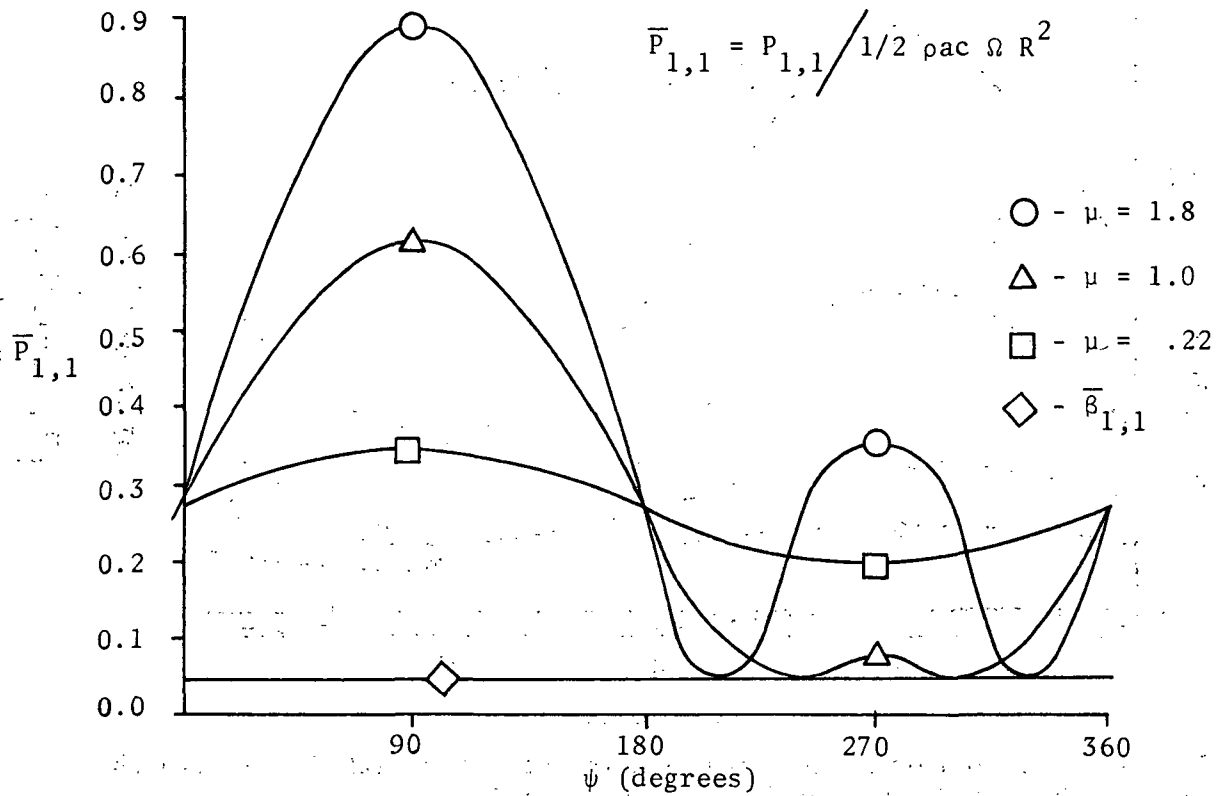
Fig. 6 Aerodynamic Damping in First Bending Mode at Various Advance Ratios, ($\kappa = 0.5$, $x_\theta = 0.0$).

$\overline{P}_{1,1} = P_{1,1} \Big/ 1/2 \, \rho a c \, \Omega \, R^2$

$\bigcirc$ — $\mu = 1.8$
$\triangle$ — $\mu = 1.0$
$\square$ — $\mu = .22$
$\diamond$ — $\overline{\beta}_{1,1}$

$\overline{m}_{1,1} = m_{1,1} \Big/ 1/2 \, \rho a c \, \Omega^2 \, R^3$

$\bigcirc$ — $\mu = 1.8$
$\triangle$ — $\mu = 1.0$
$\square$ — $\mu = .22$
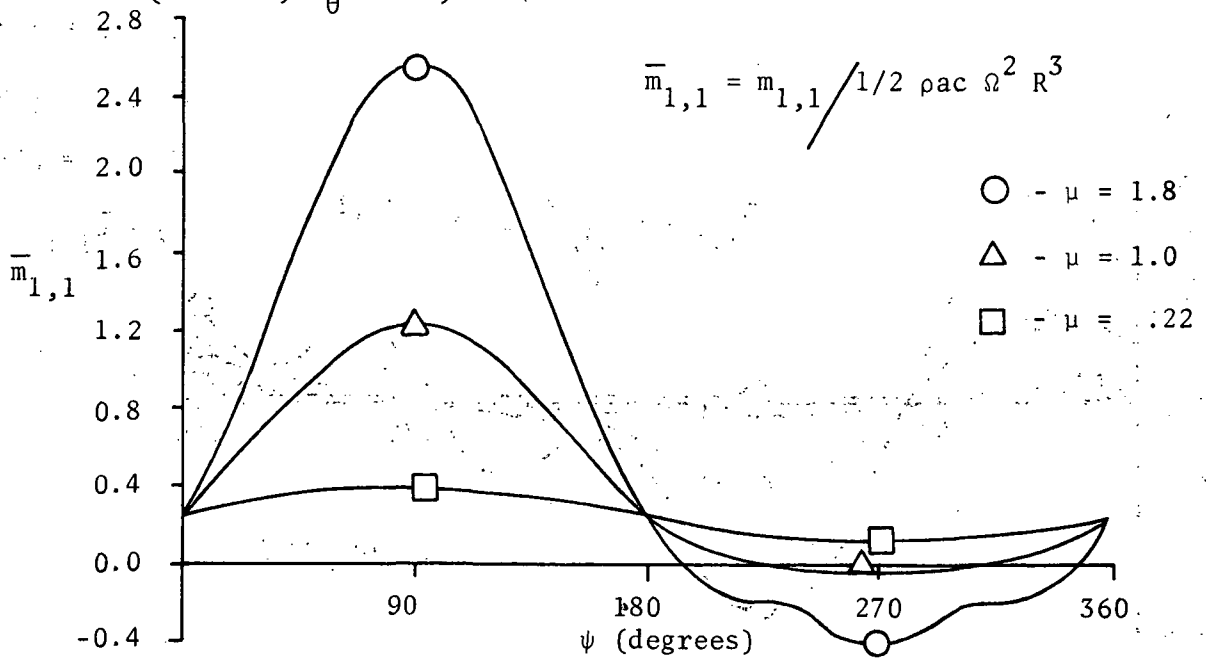
Fig. 7 Aerodynamic Stiffness Coupling of First Torsional and First Bending Modes at Various Advance Ratios, ($\kappa = 0.5$, $x_\theta = 0.0$).

30
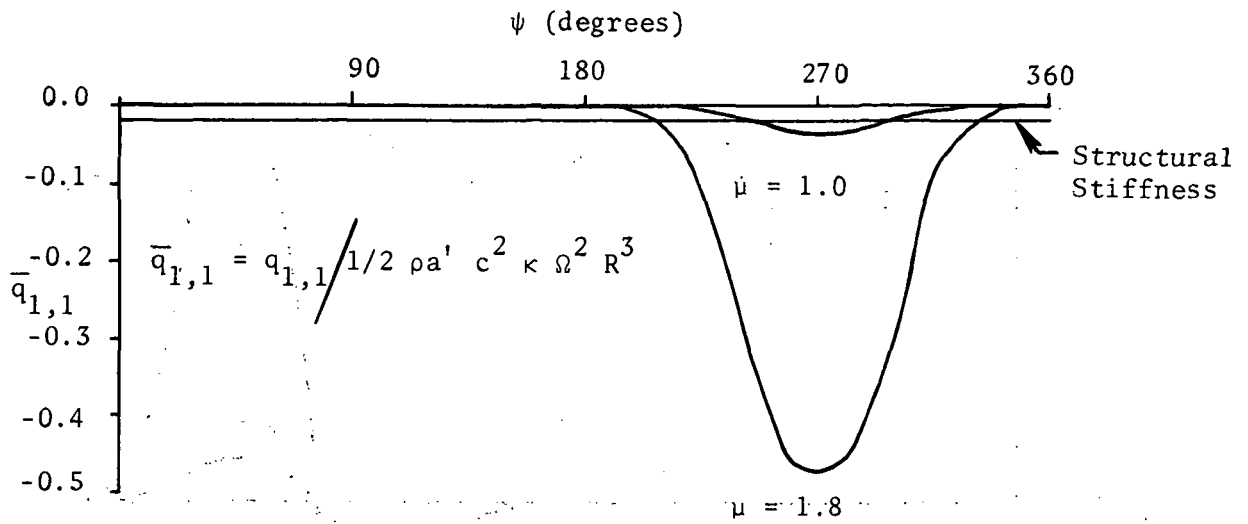
Fig. 8 Aerodynamic Stiffness for First Torsional Mode with Various Advance Ratios, (κ = 0.5, x_θ = 0.0).

$$\overline{q}_{1,1} = q_{1,1} \Big/ 1/2 \, \rho a' \, c^2 \, \kappa \, \Omega^2 \, R^3$$

$\mu = 1.0$

Structural Stiffness

$\mu = 1.8$
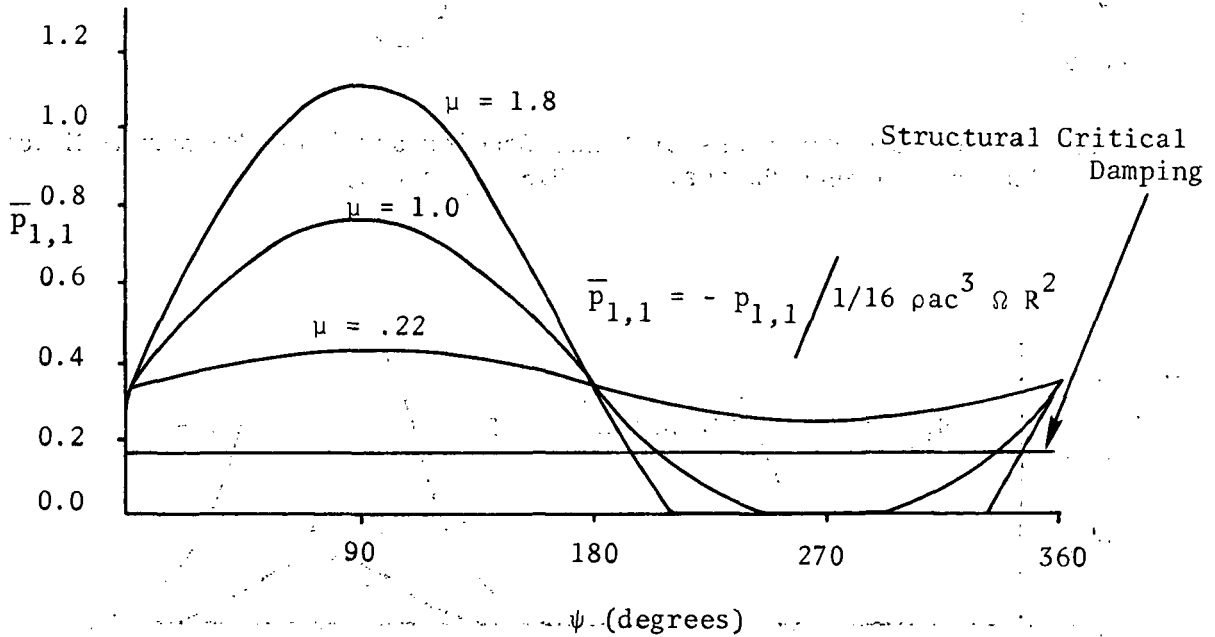
Fig. 9 Aerodynamic Damping for First Torsional Mode with Various Advance Ratios, (κ = 0.5, x_θ = 0.0).

$$\overline{p}_{1,1} = - p_{1,1} \Big/ 1/16 \, \rho a c^3 \, \Omega \, R^2$$

$\mu = 1.8$

$\mu = 1.0$

$\mu = .22$

Structural Critical Damping
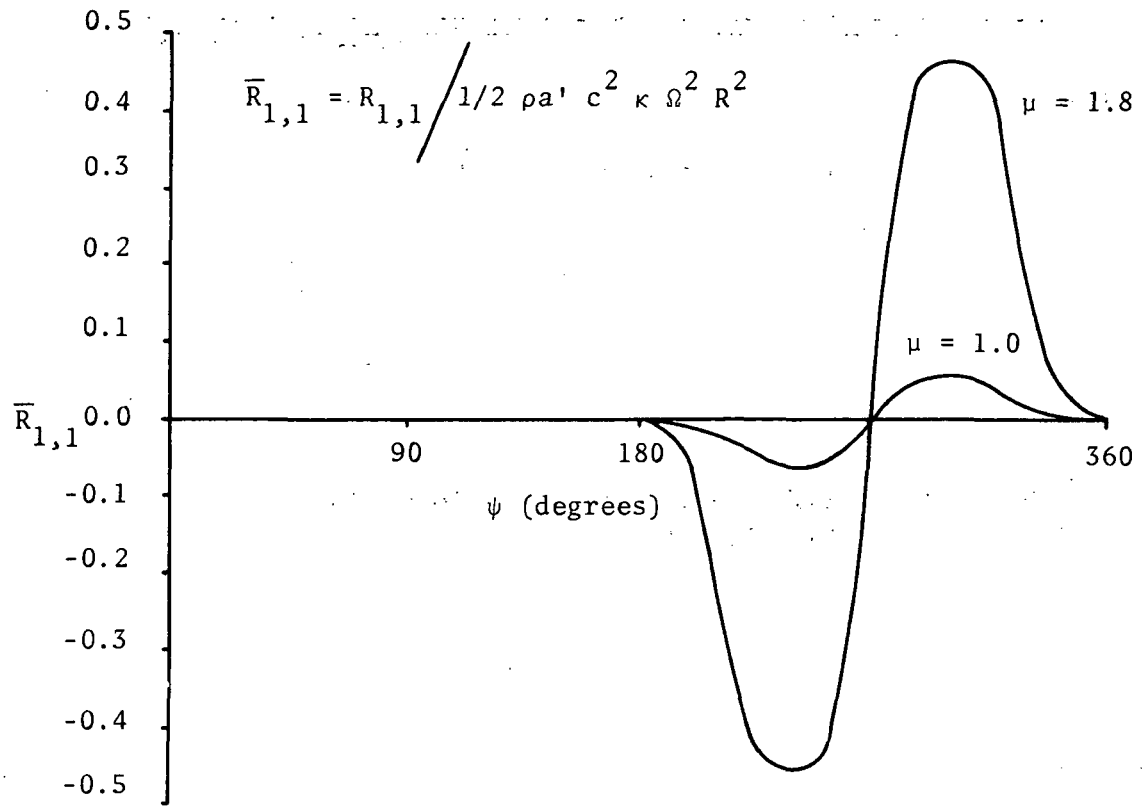
Fig. 10   Aerodynamic Stiffness of First Bending and First Torsional Modes at Various Advance Ratios, (κ = 0.5, x_θ = 0.0).
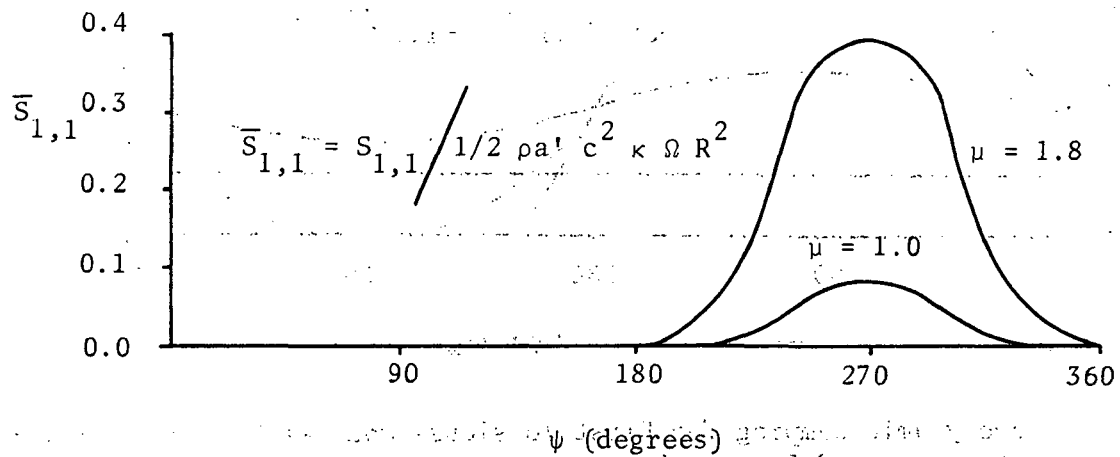
Fig. 11   Aerodynamic Damping Coupling of First Bending and First Torsional Modes at Various Advance Ratios, (κ = 0.5, x_θ = 0.0).
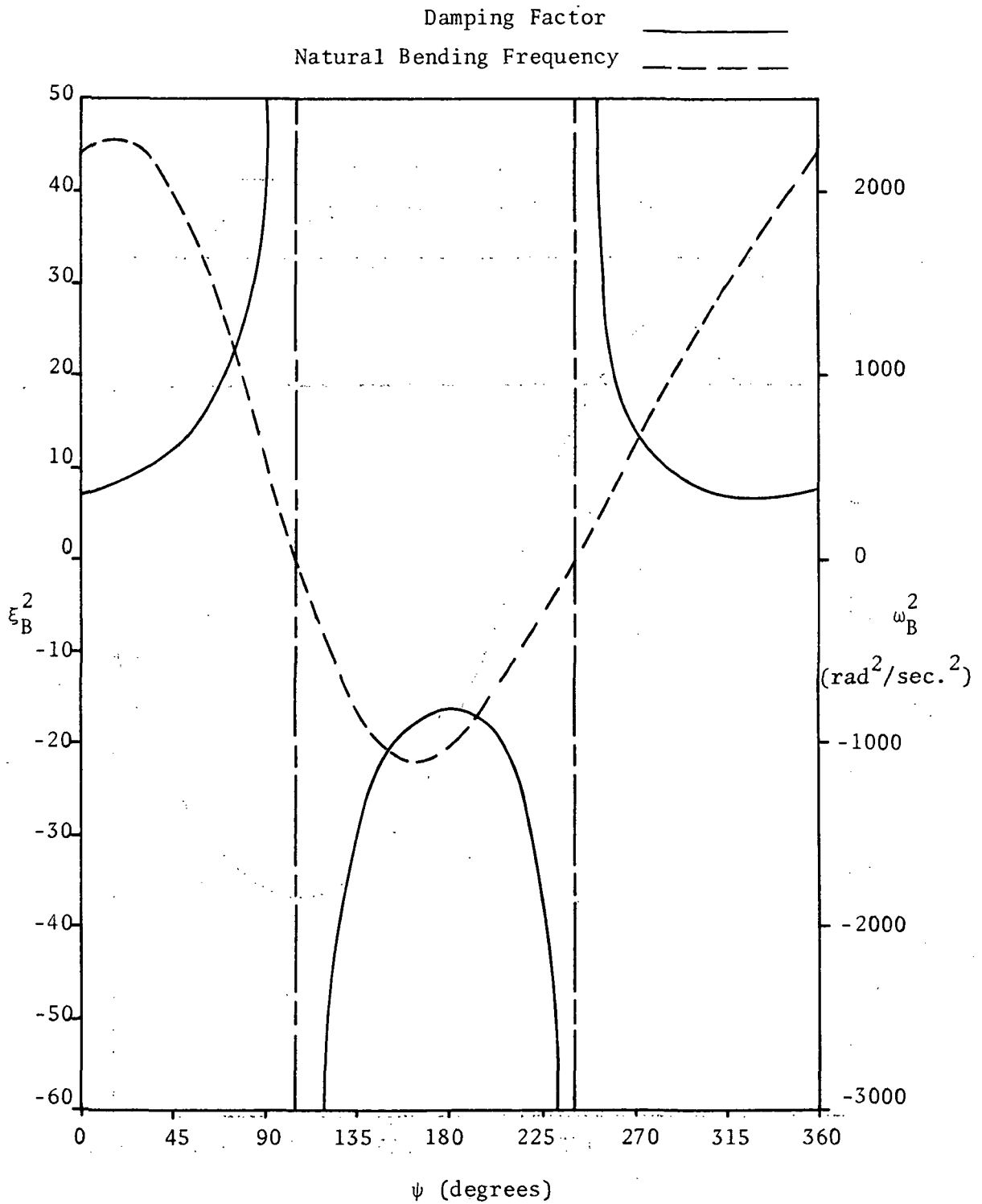
Fig. 12 Variation of Natural Bending Frequency and Damping Ratio with Blade Azimuth Positions, ($\mu = 0.22$, $\kappa = 0.5$, $x_\theta = 0.0$).
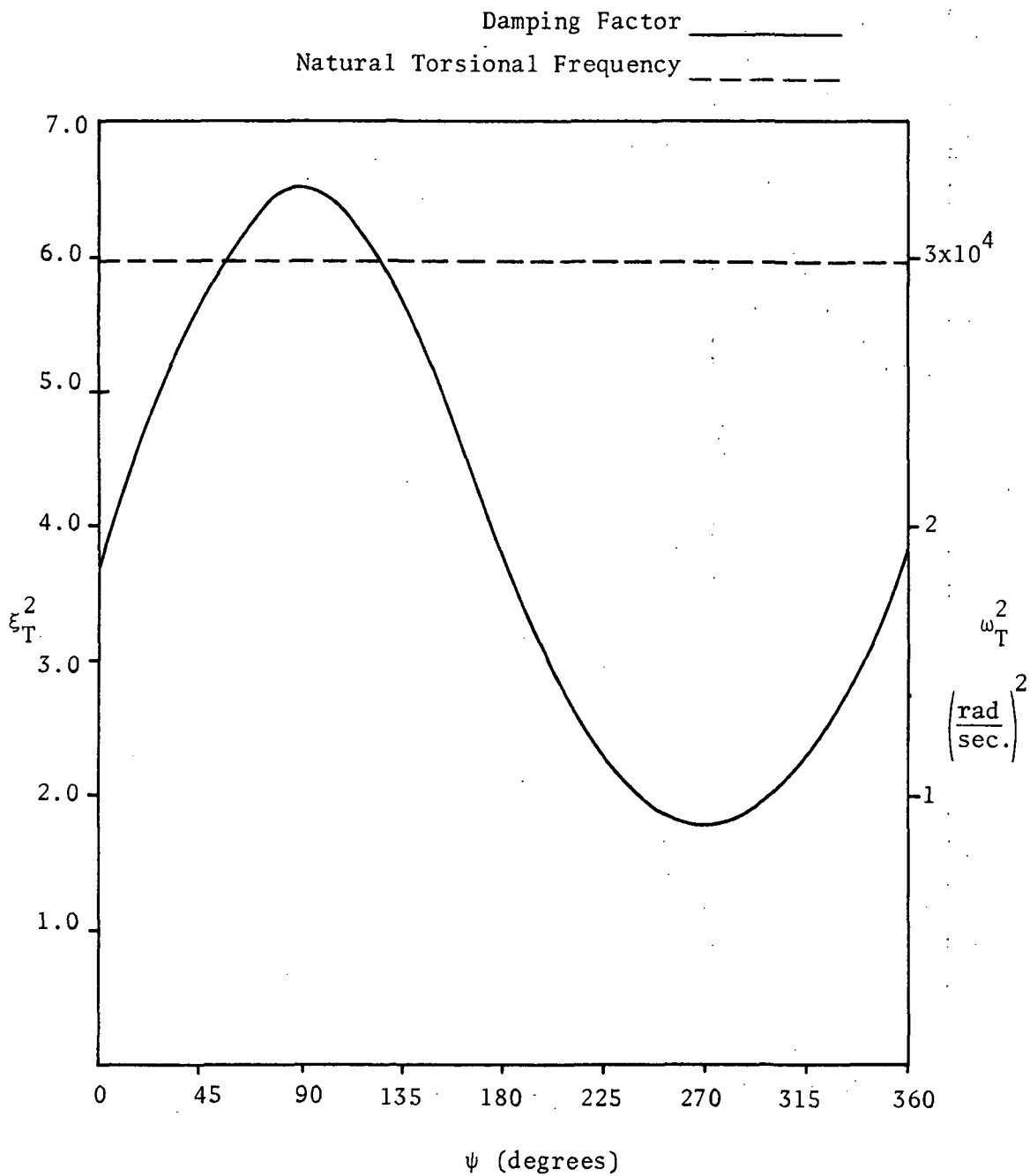
Fig. 13 Variation of Natural Torsional Frequency and Damping Ratio with Blade Azimuth Positions, (μ = 0.22, κ = 0.5, x_θ = 0.0).

Fig. 14 Variation of Coupling Ratios for the Torsional and Bending Modes with Blade Azimuth Positions, ($\mu = 0.22$, $\kappa = 0.5$, $x_\theta = 0.0$).
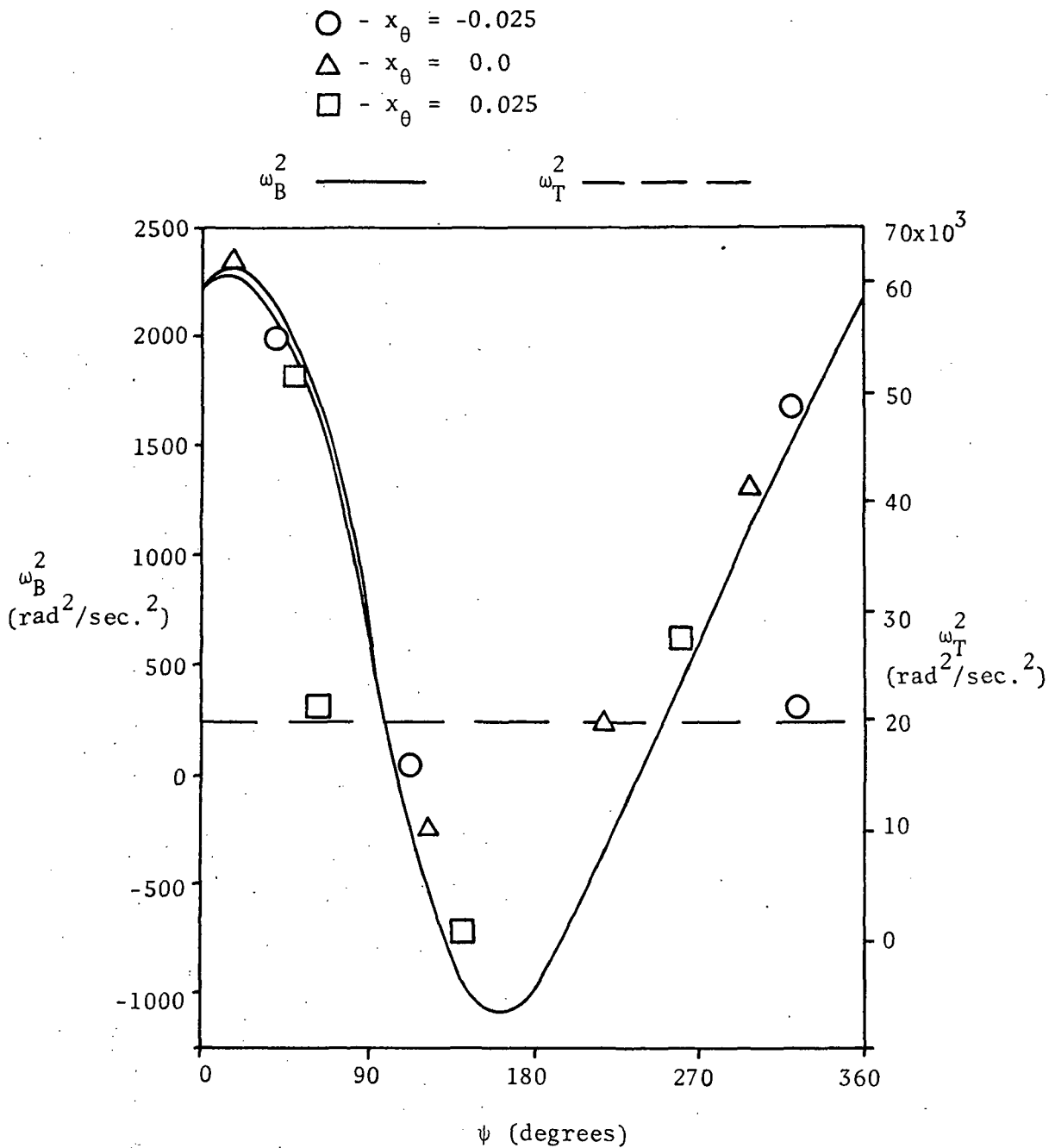
Fig. 15 Variation of Natural Bending and Torsional Frequencies with Blade Azimuth Positions for Various Eccentricities between Elastic and Mass Axes, ($\mu = 0.22$, $\kappa = 0.5$).
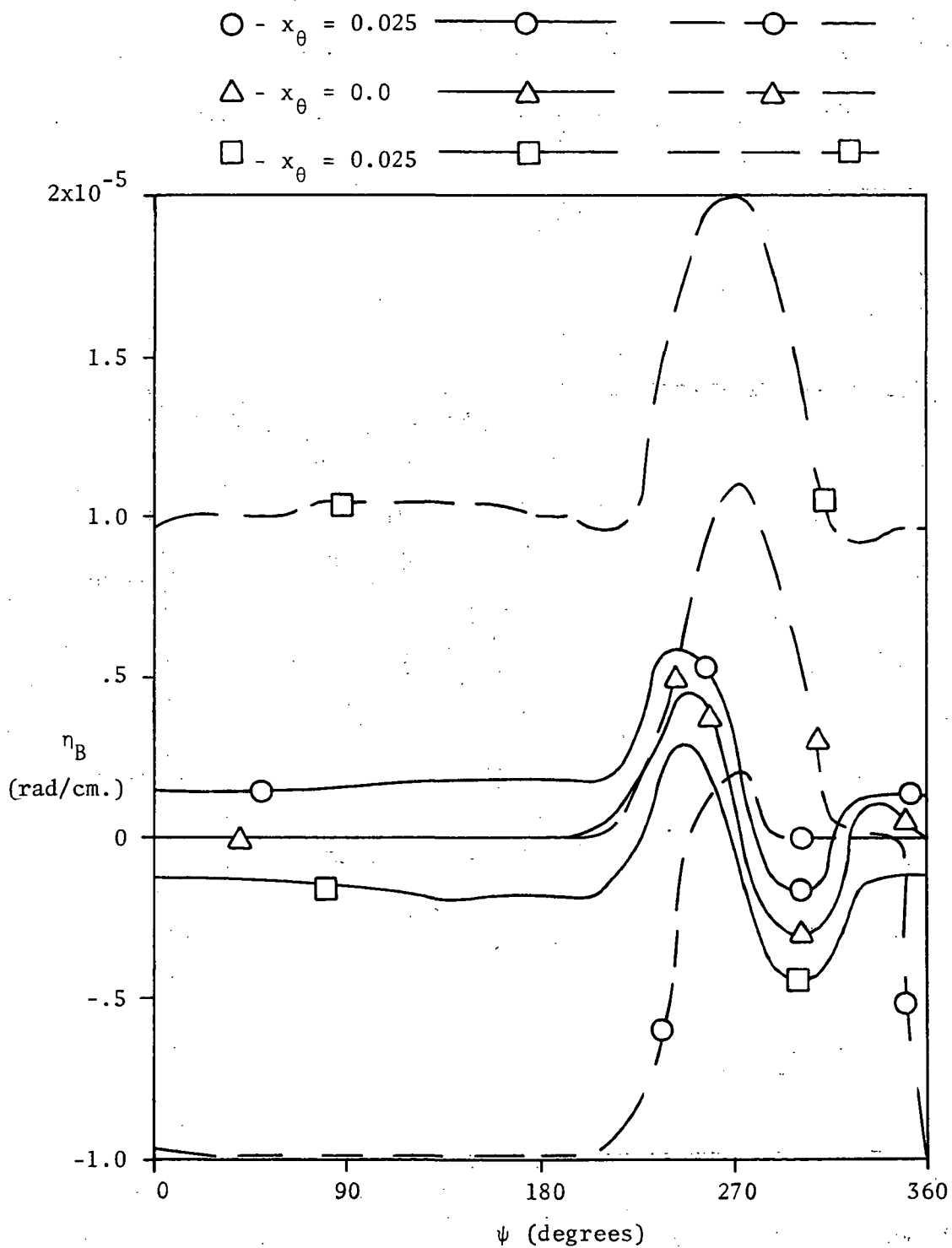
Fig. 16 Variation of Coupling Ratios for the Bending Mode with Blade
Azimuth Positions for Various Eccentricities between Elastic
and Mass Axes, ($\mu = 0.22$, $\kappa = 0.5$).
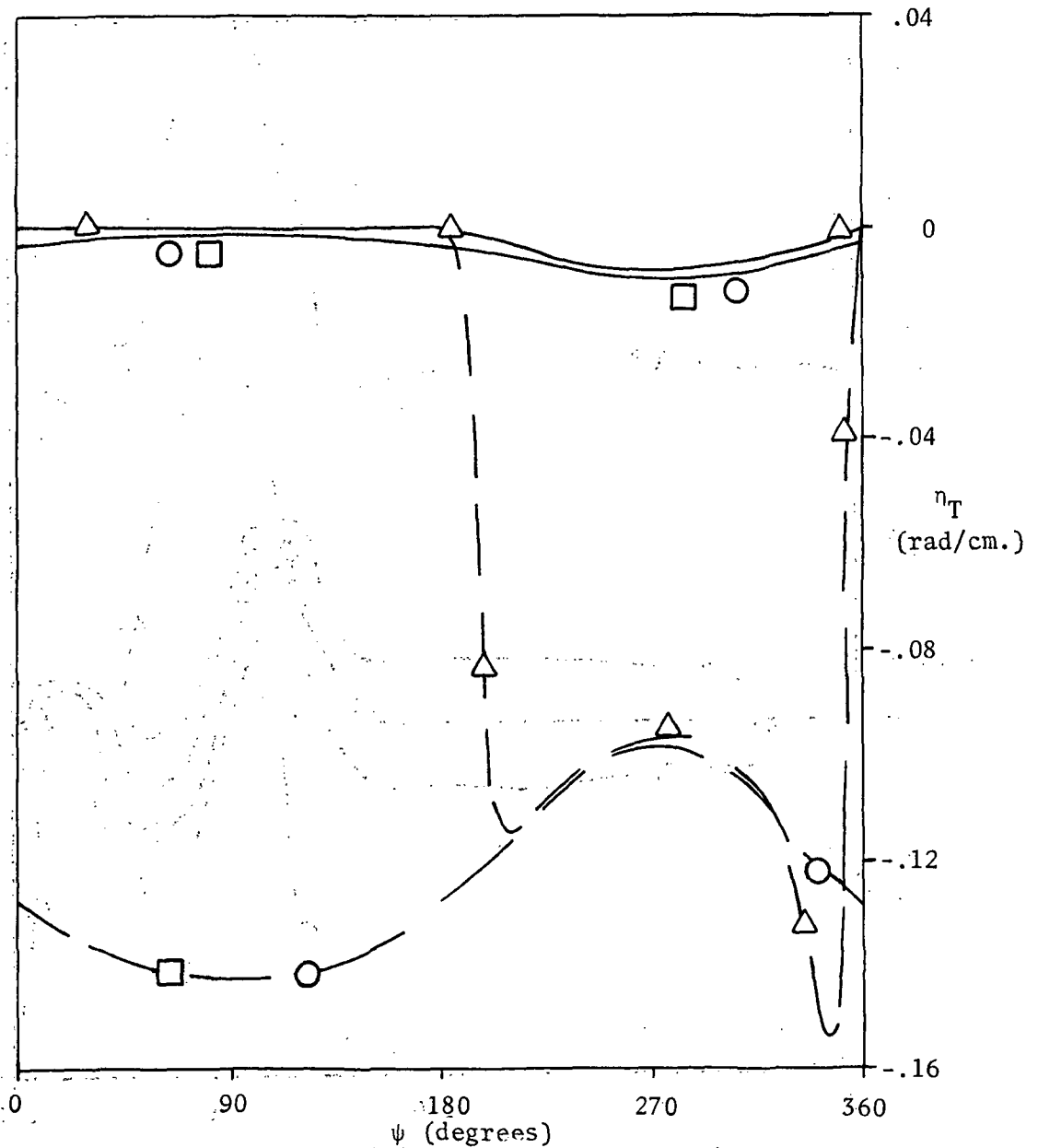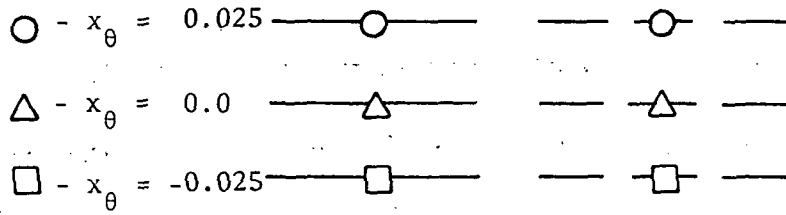
Fig. 17 Variation of Coupling Ratios for the Torsional Mode with Blade
Azimuth Positions for Various Eccentricities between Elastic
and Mass Axes, ($\mu = 0.22$, $\kappa = 0.5$).
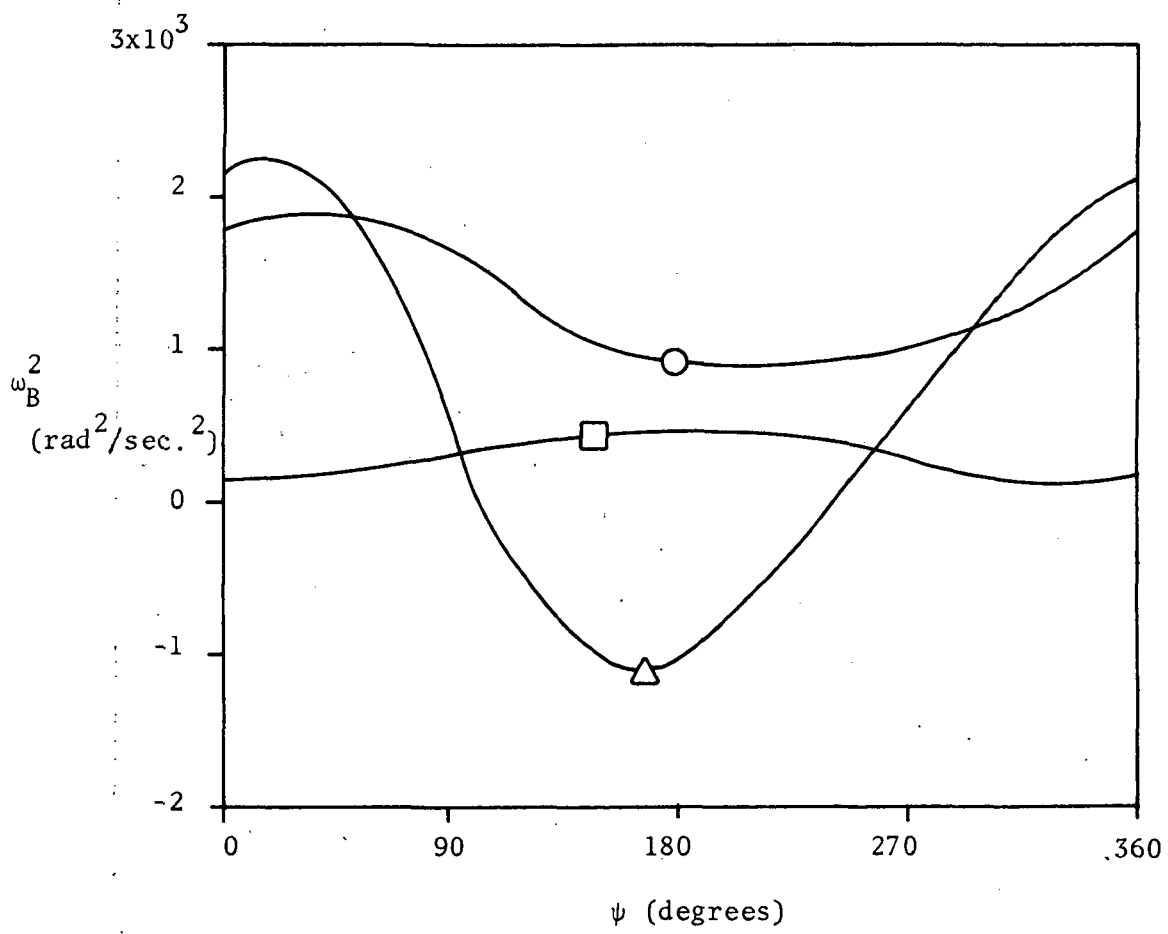
Fig. 18 Variation of Natural Bending Frequency with Blade Azimuth
Positions for Various Eccentricities between Elastic and Aero-
dynamic Axes, (μ = 0.22, x_θ = 0.0).

39
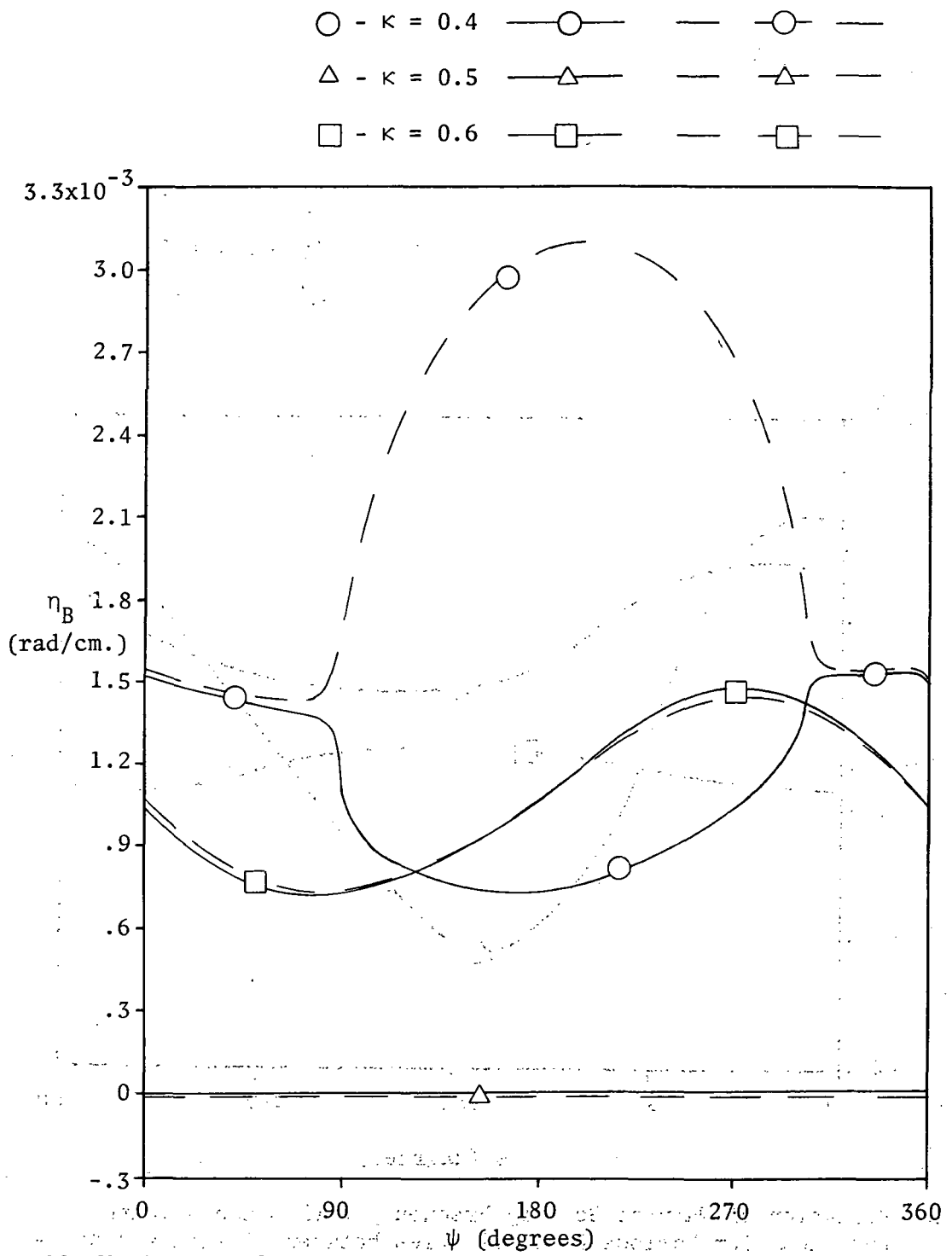
Fig. 19 Variation of Coupling Ratios for the Bending Mode with Blade
Azimuth Positions for Various Eccentricities between Elastic
and Aerodynamic Axes, ($\mu = 0.22$, $x_\theta = 0$).

40
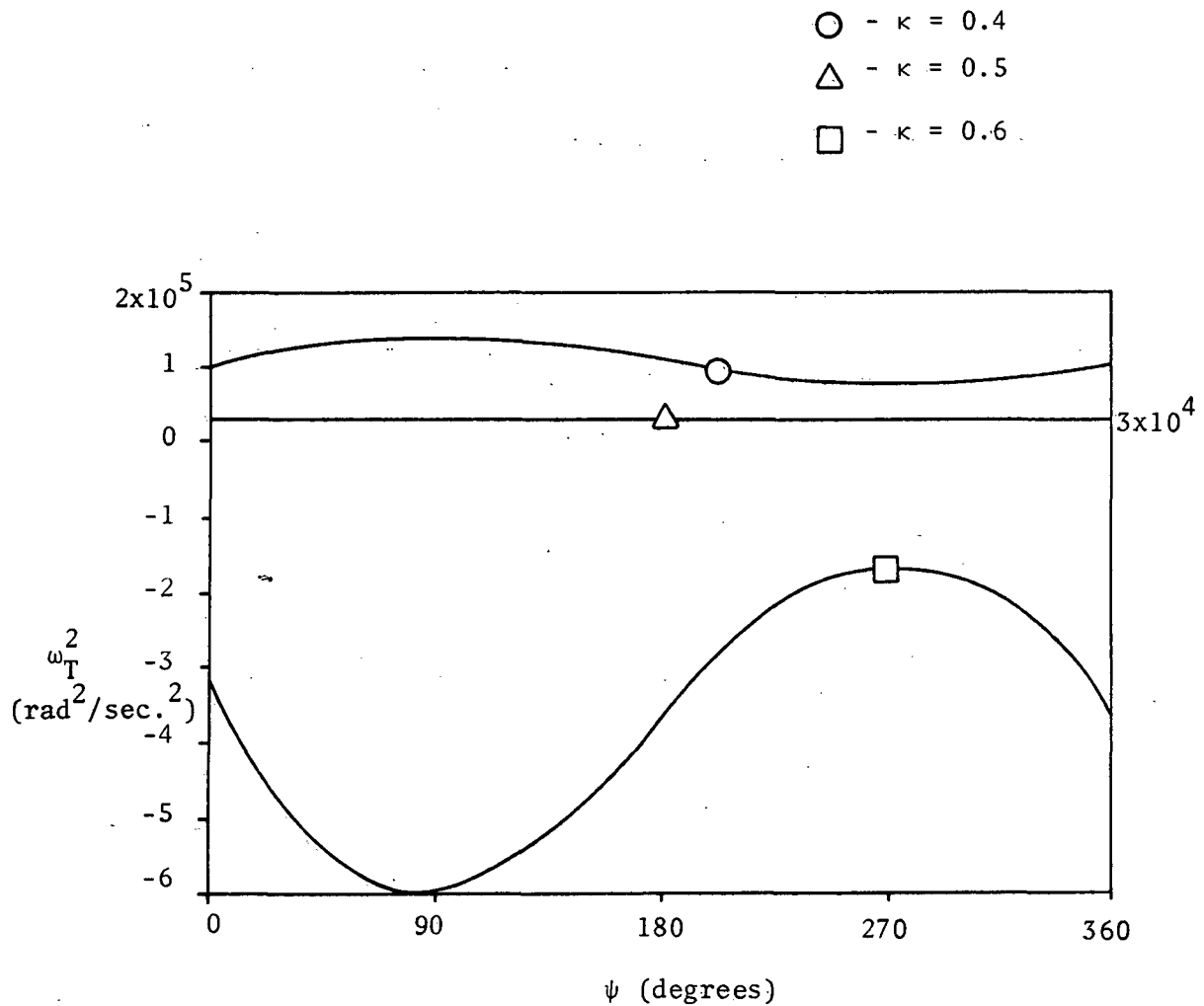
Fig. 20 Variation of Natural Torsional Frequency with Blade Azimuth
Positions for Various Eccentricities between Elastic and Aero-
dynamic Axes, (μ = 0.22, x_θ = 0.0).
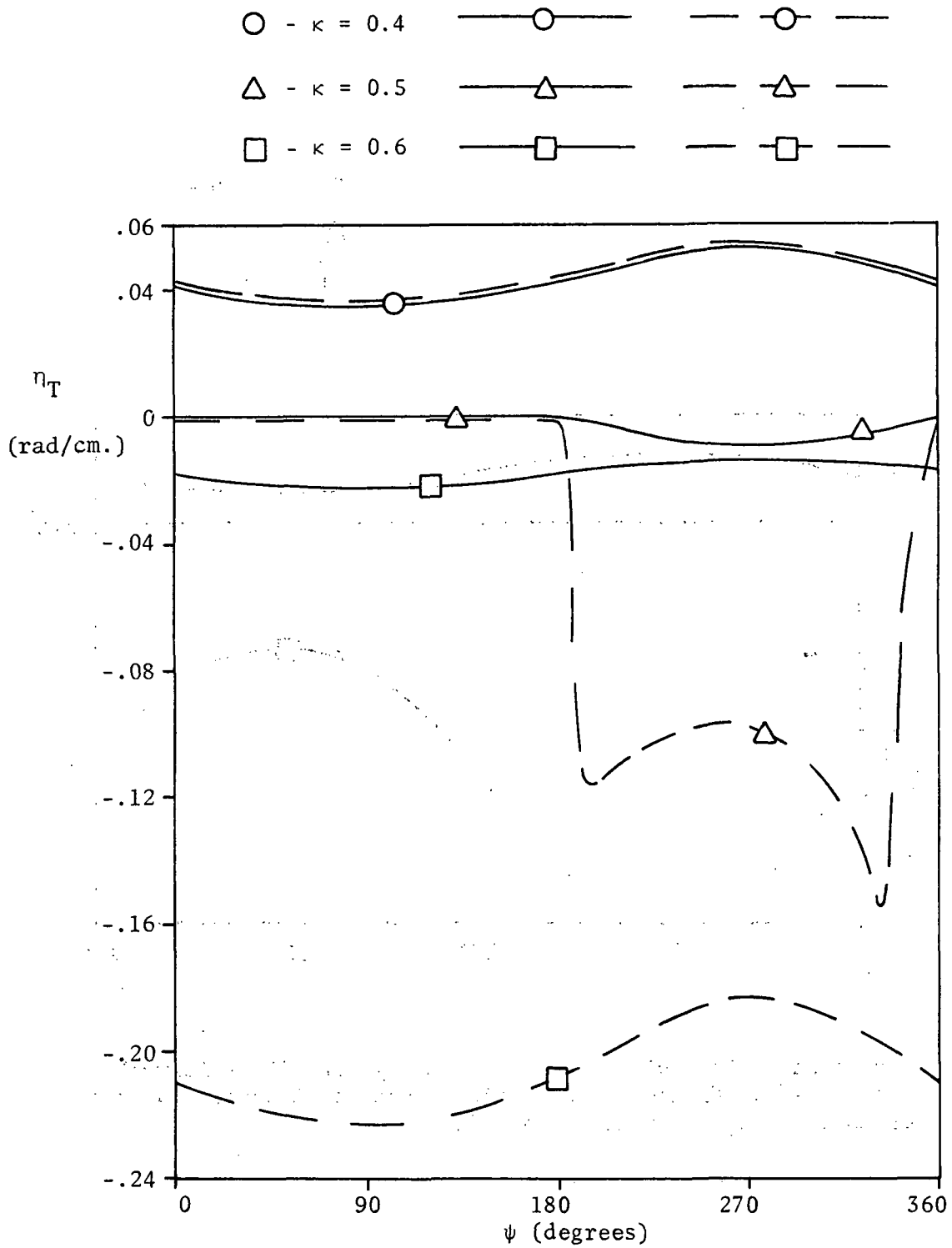
Fig. 21 Variation of Coupling Ratios for the Torsional Mode with Blade
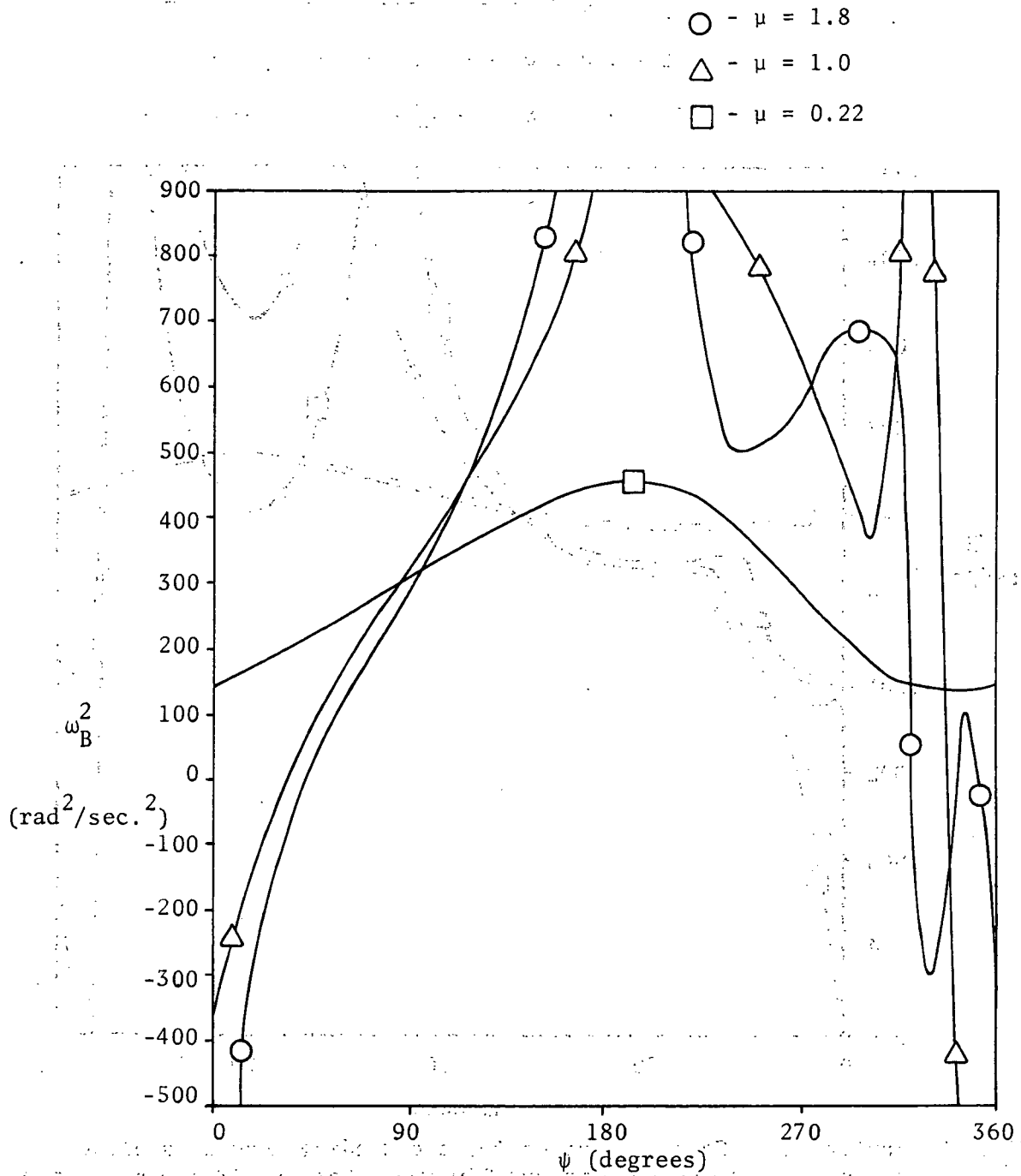Azimuth Positions for Various Eccentricities between Elastic
and Aerodynamic Axes, (μ = 0.22, x_θ = 0.0).

42
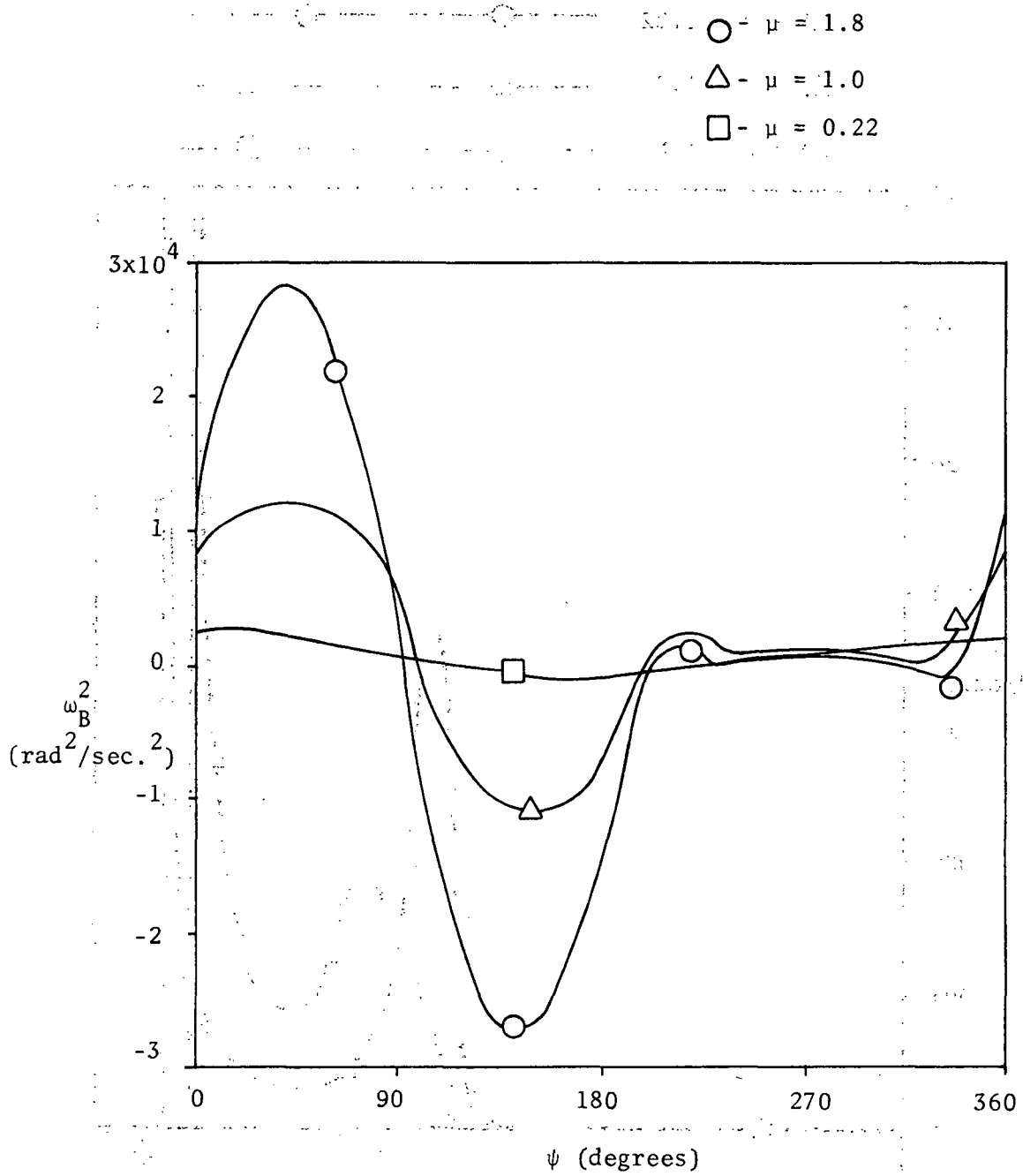
Fig. 22 Variation of Natural Bending Frequency with Blade Azimuth
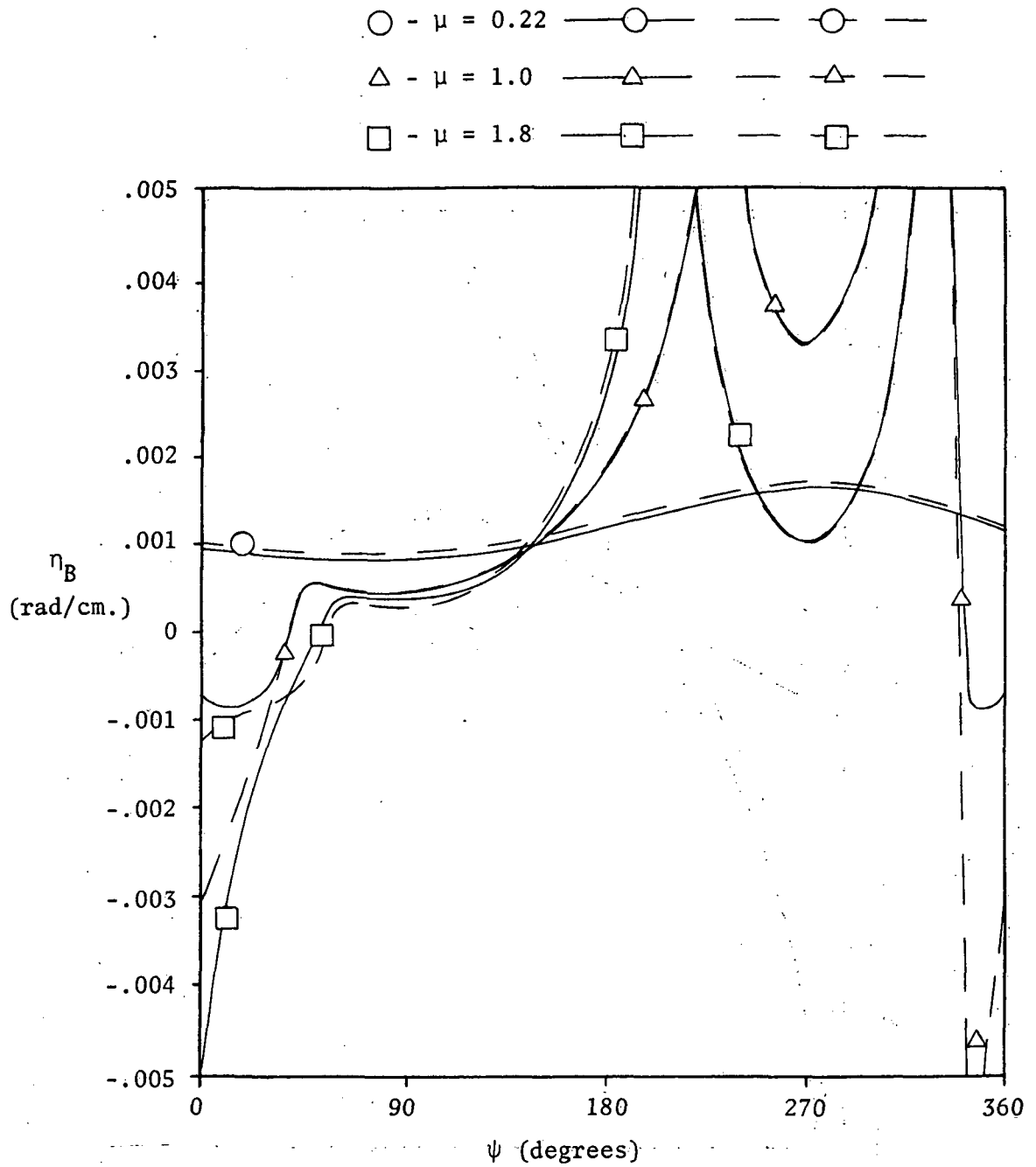Positions for Various Tip-Speed Ratios, (κ = 0.5, x_θ = 0.0).
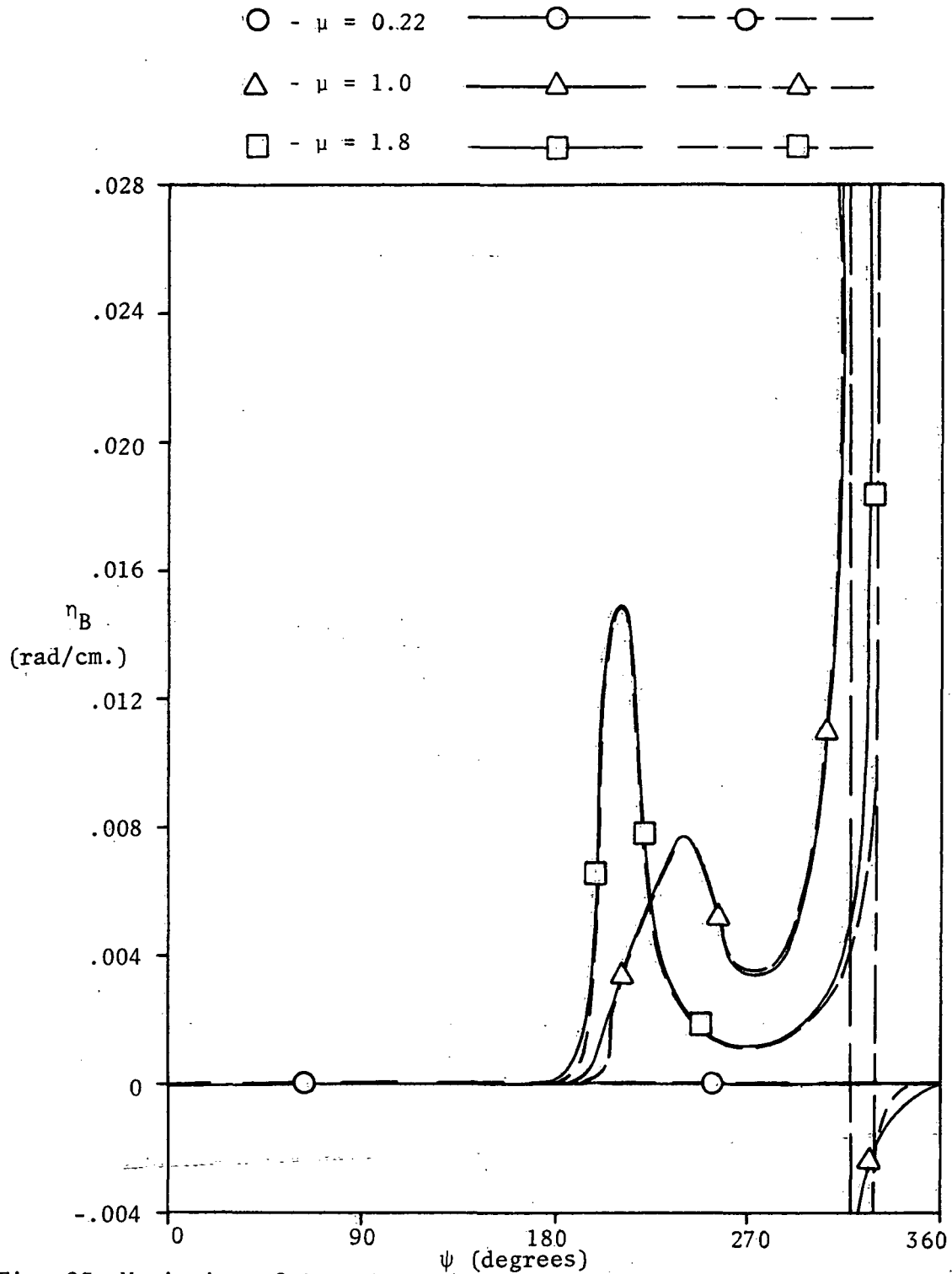
Fig. 23 Variation of Coupling Ratios for the Bending Mode with Blade Azimuth Positions for Various Tip-Speed Ratios, ($\kappa = 0.5$, $x_\theta = 0.0$).
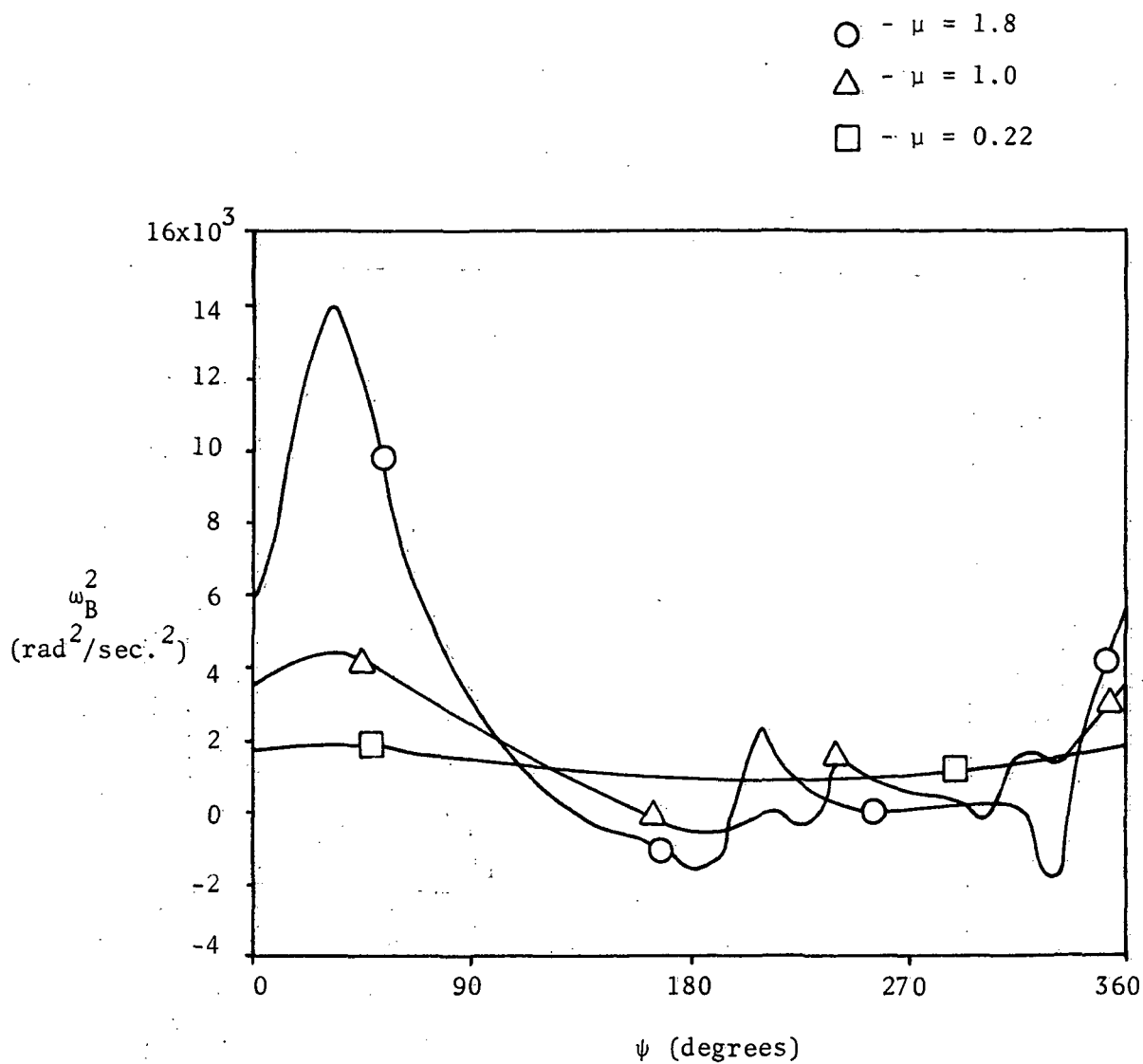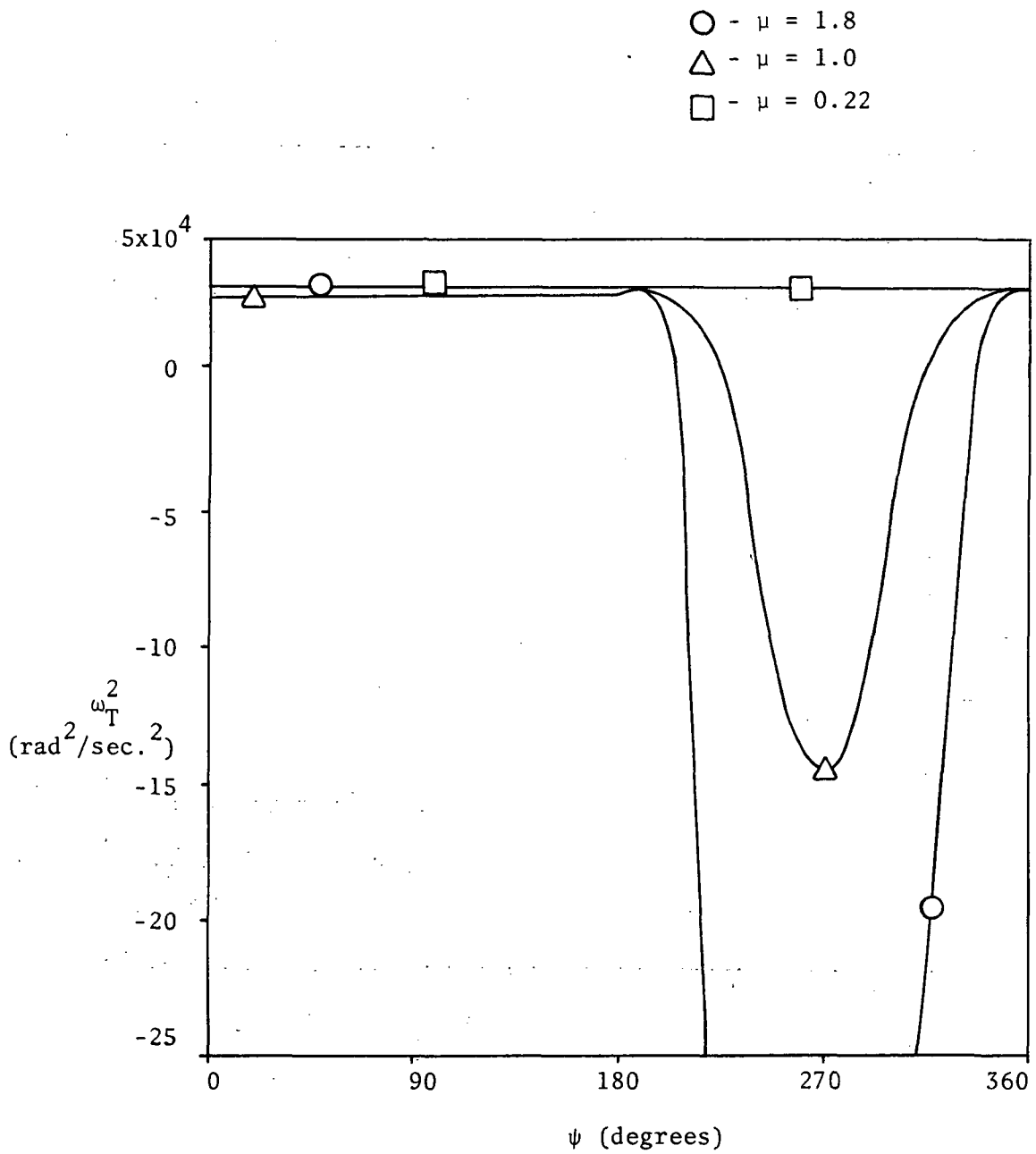
Fig. 24 Variation of Natural Bending Frequency with Blade Azimuth Positions for Various Tip-Speed Ratios, ($\kappa = 0.4$, $x_\theta = 0.0$).
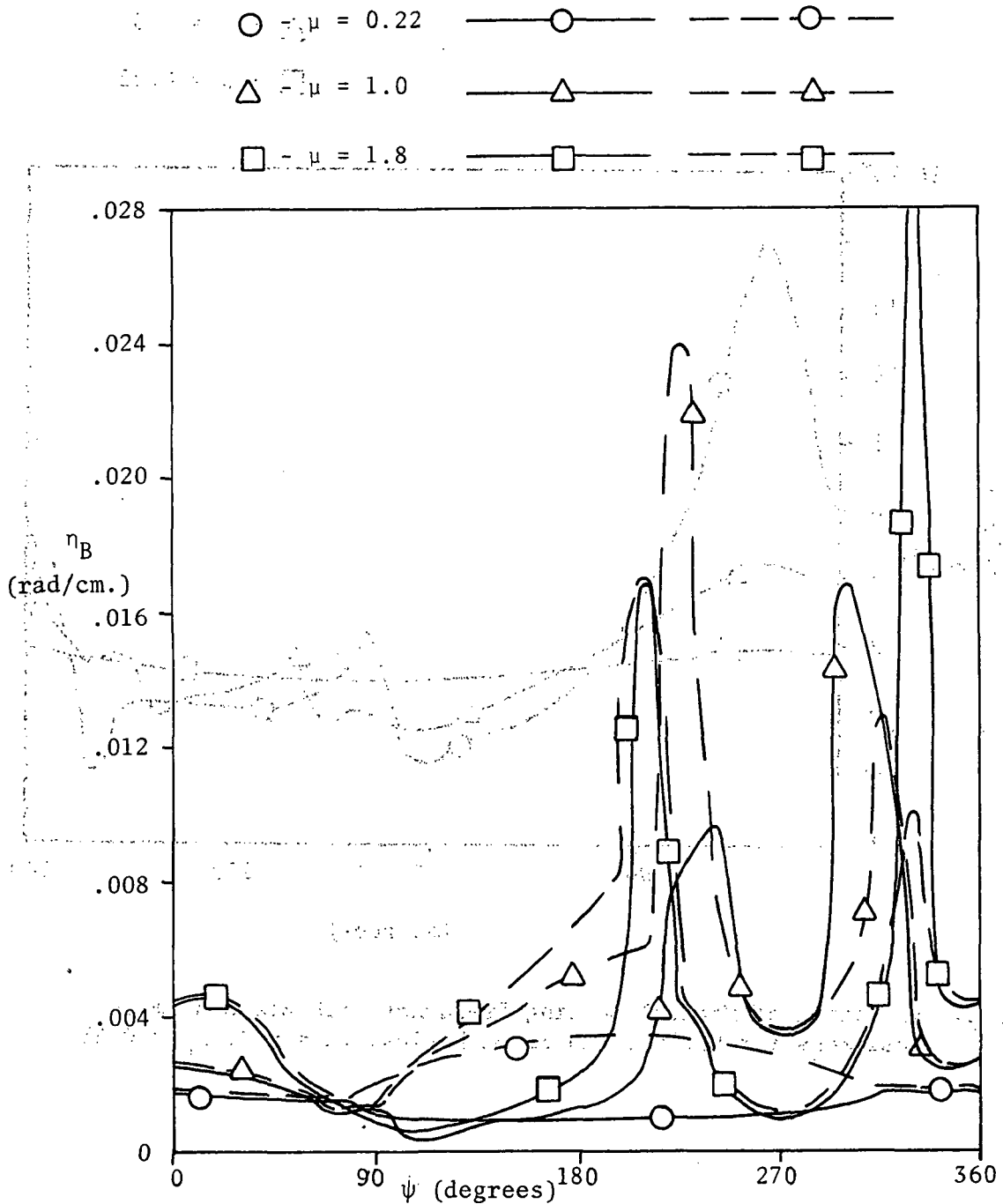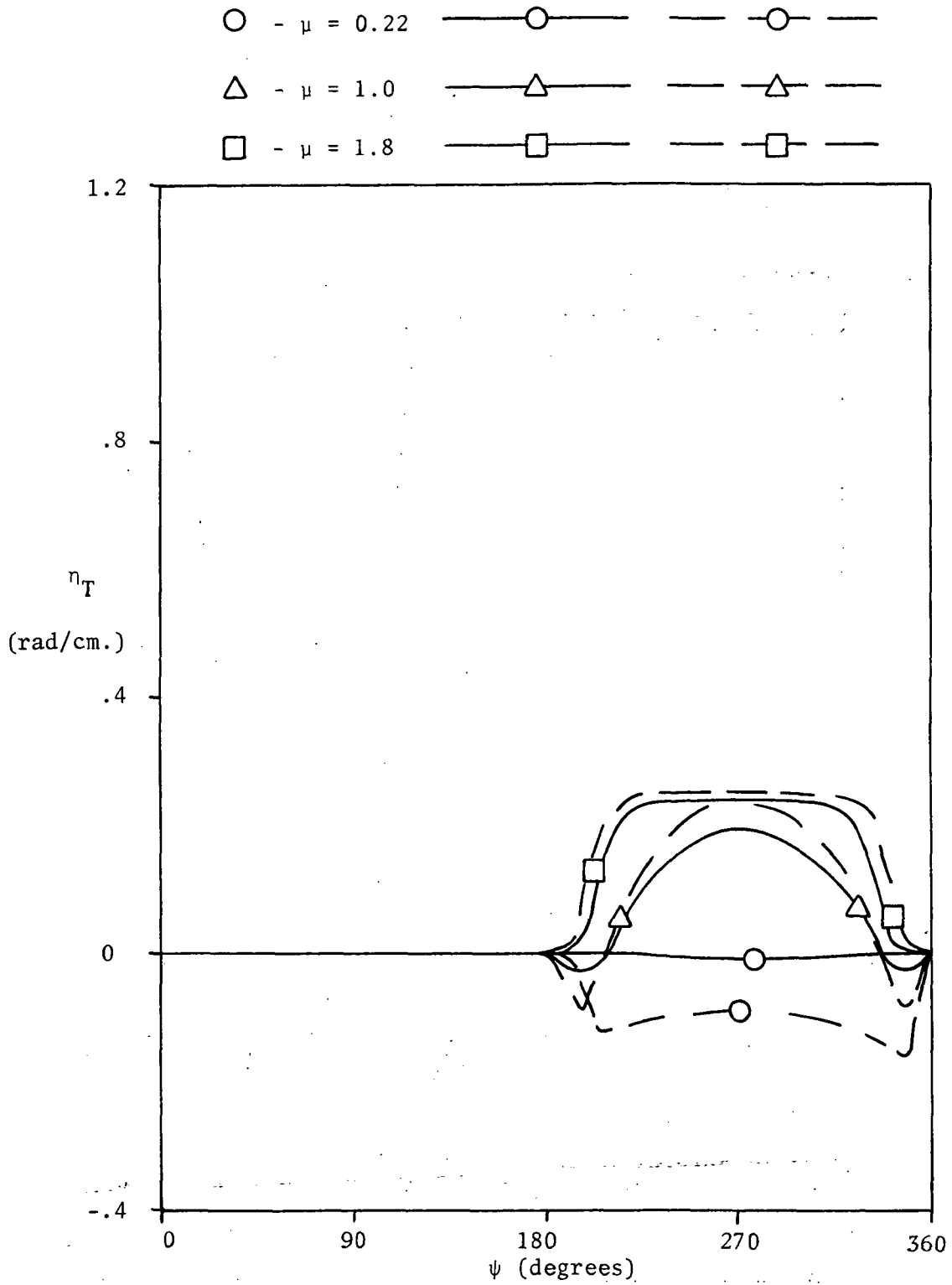
Fig. 25 Variation of Coupling Ratios for the Bending Mode with Blade
Azimuth Positions for Various Tip-Speed Ratios, ($\kappa = 0.4$,
$x_\theta = 0.0$).

Fig. 26 Variation of Natural Bending Frequency with Blade Azimuth
Positions for Various Tip-Speed Ratios, ($\kappa = 0.6$, $x_\theta = 0.0$).

Fig. 27 Variation of Coupling Ratios for the Bending Mode with Blade
Azimuth Positions for Various Tip-Speed Ratios, ($\kappa = 0.6$, $x_\theta = 0$).
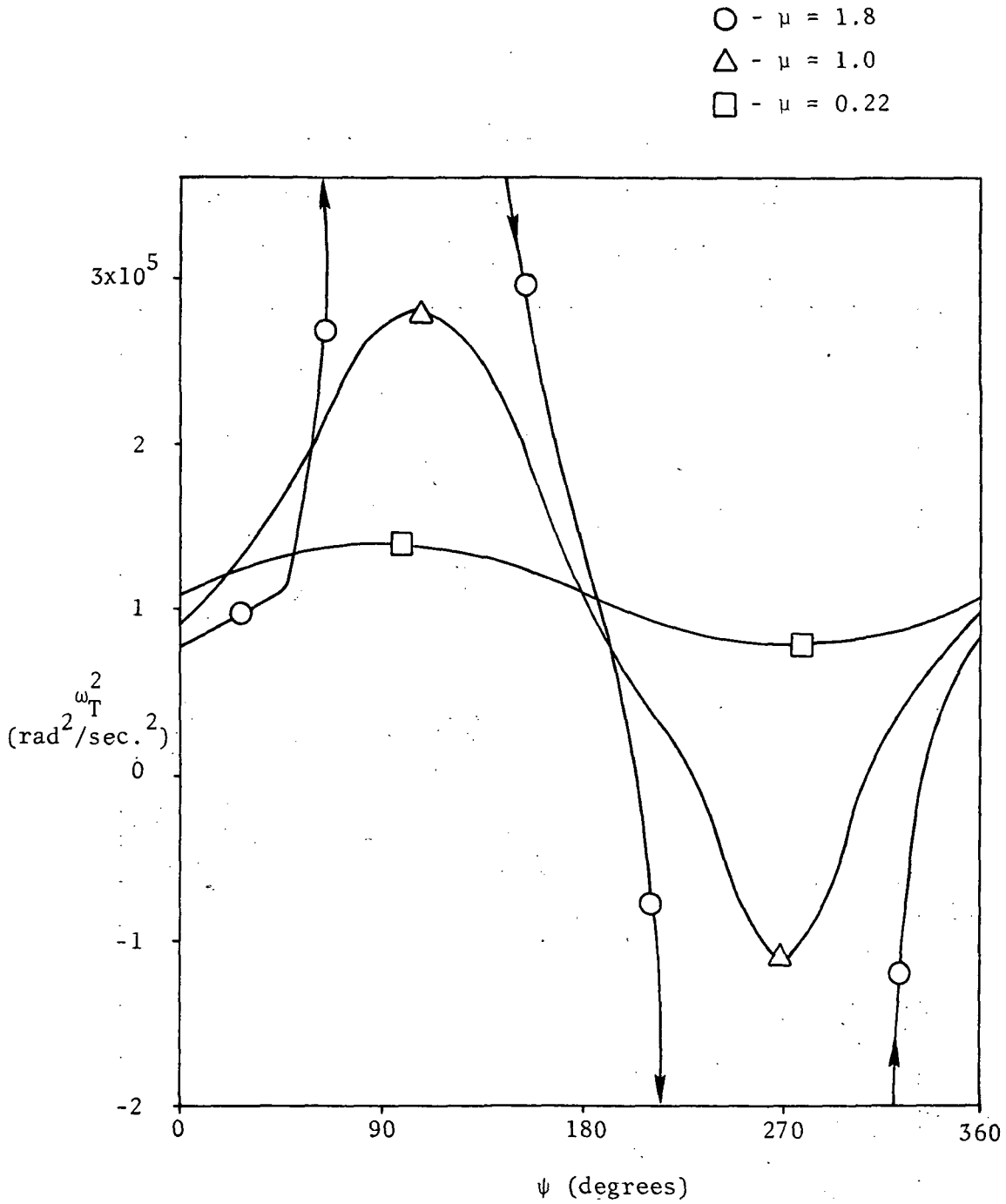
Fig. 28 Variation of Natural Torsional Frequency with Blade Azimuth
        Positions for Various Tip-Speed Ratios, (κ = 0.5, x_θ = 0.0).

Fig. 29 Variation of Coupling Ratios for Torsional Mode with Blade Azimuth Positions for Various Tip-Speed Ratios, ($\kappa = 0.5$, $x_\theta = 0.0$).

Fig. 30 Variation of Natural Torsional Frequency with Blade Azimuth
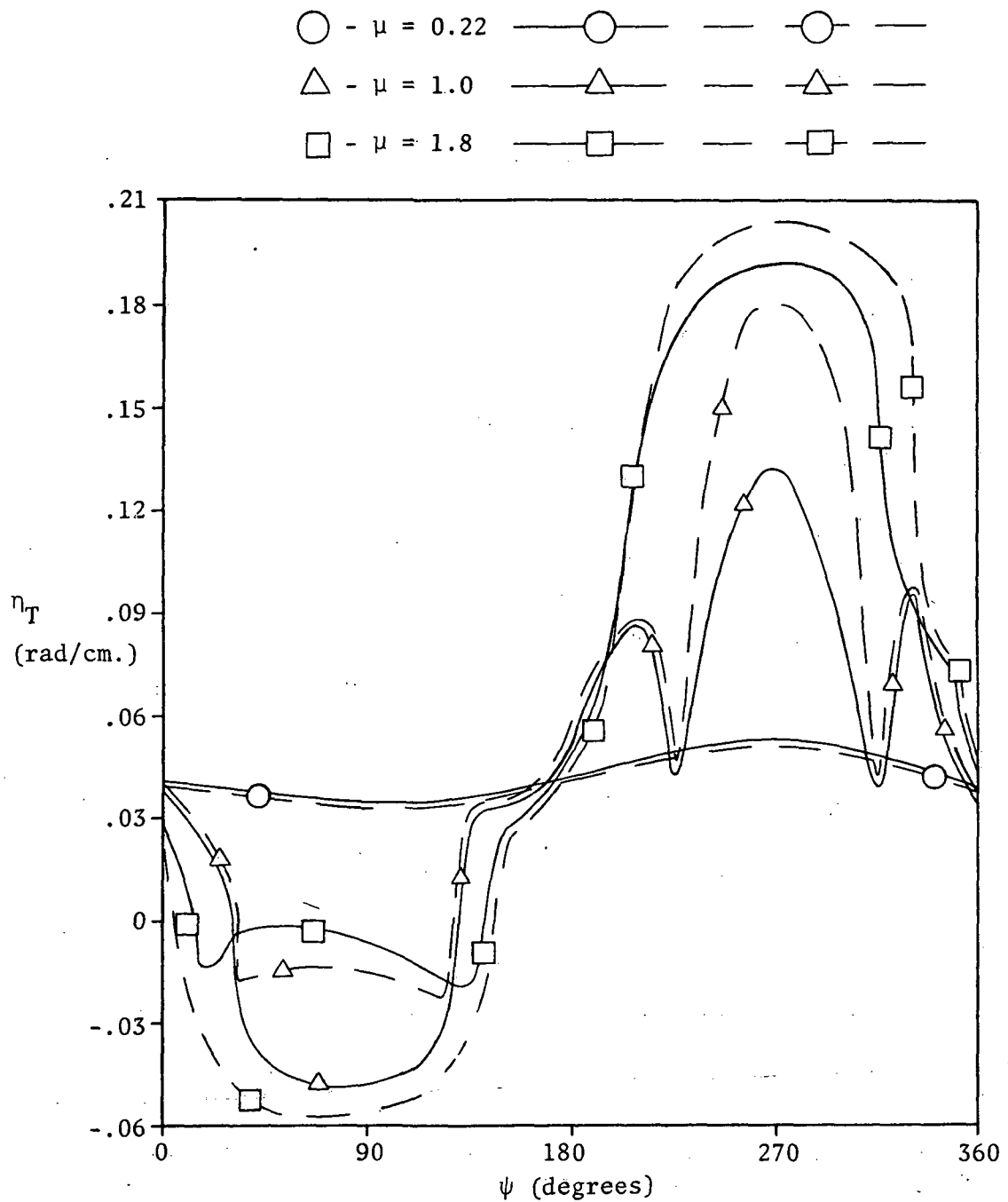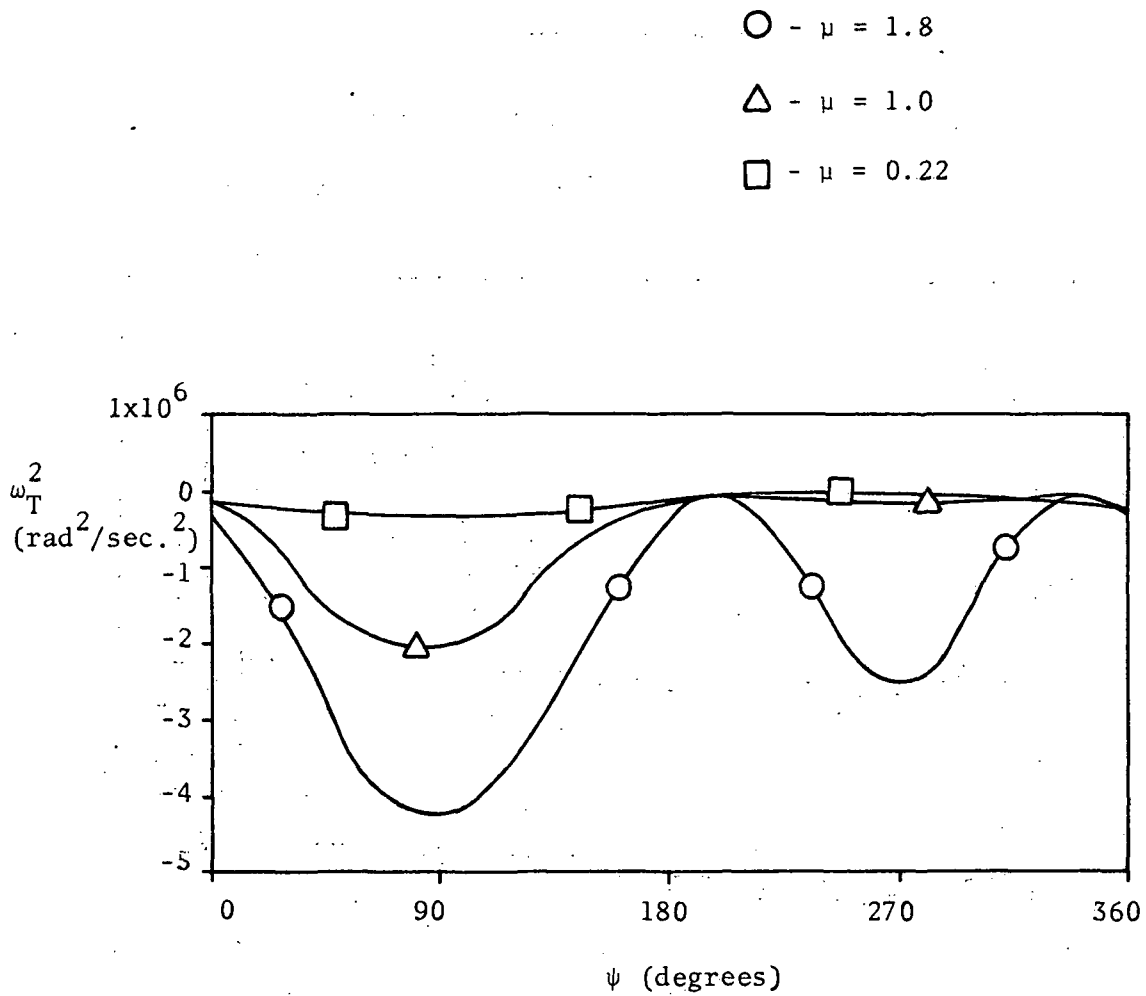Positions for Various Tip-Speed Ratios, ($\kappa = 0.4$, $x_\theta = 0.0$).

Fig. 31 Variation of Coupling Ratios for the Torsional Mode with Blade
Azimuth Positions for Various Tip-Speed Ratios, (κ = 0.4, x_θ = 0).

Fig. 32 Variation of Natural Torsional Frequency with Blade Azimuth
Positions for Various Tip-Speed Ratios, (κ = 0.6, x_θ = 0.0).
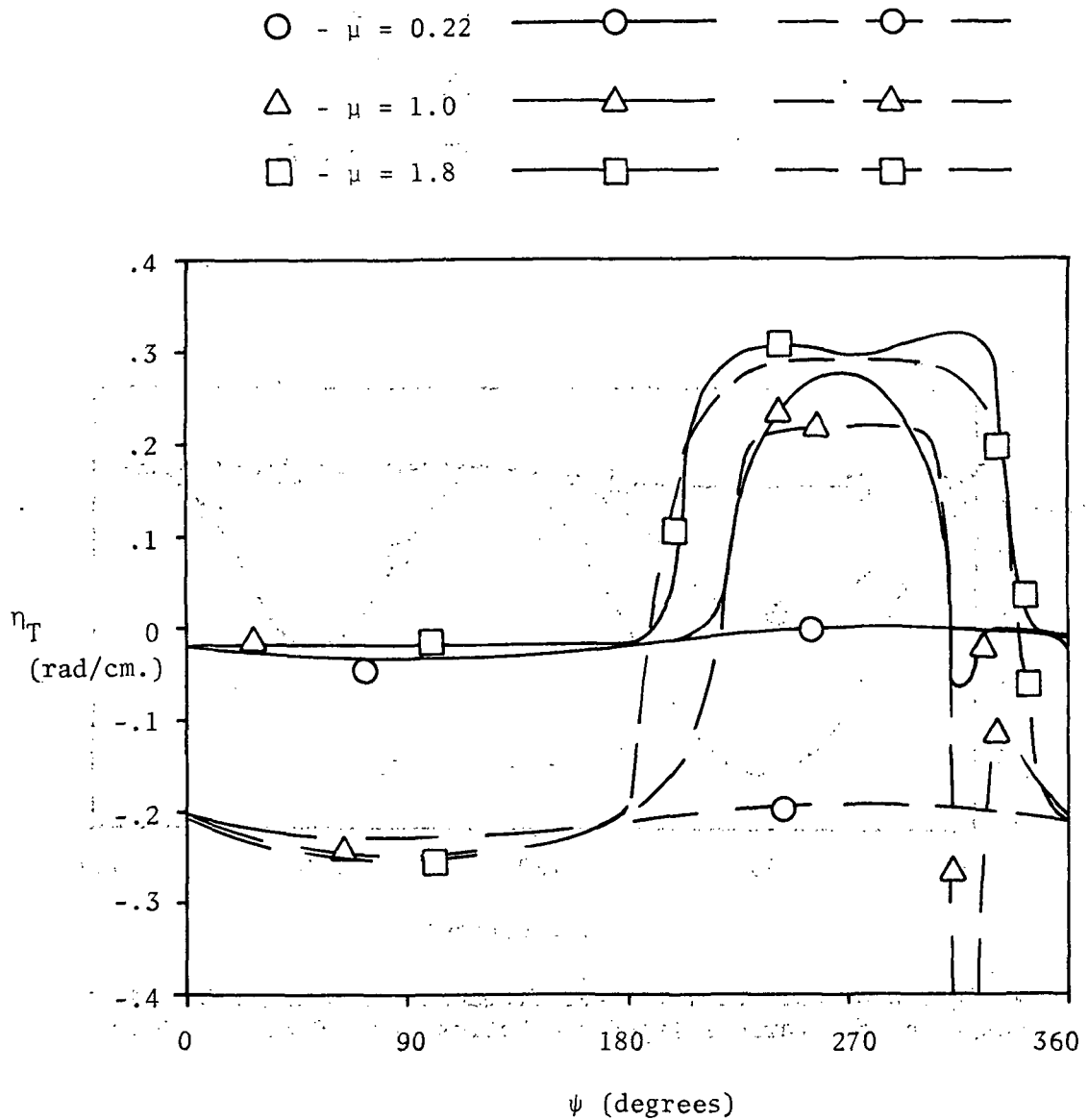
Fig. 33 Variation of Coupling Ratios for the Torsional Mode with Blade Azimuth Positions for Various Tip-Speed Ratios, ($\kappa = 0.6$, $x_\theta = 0.0$).
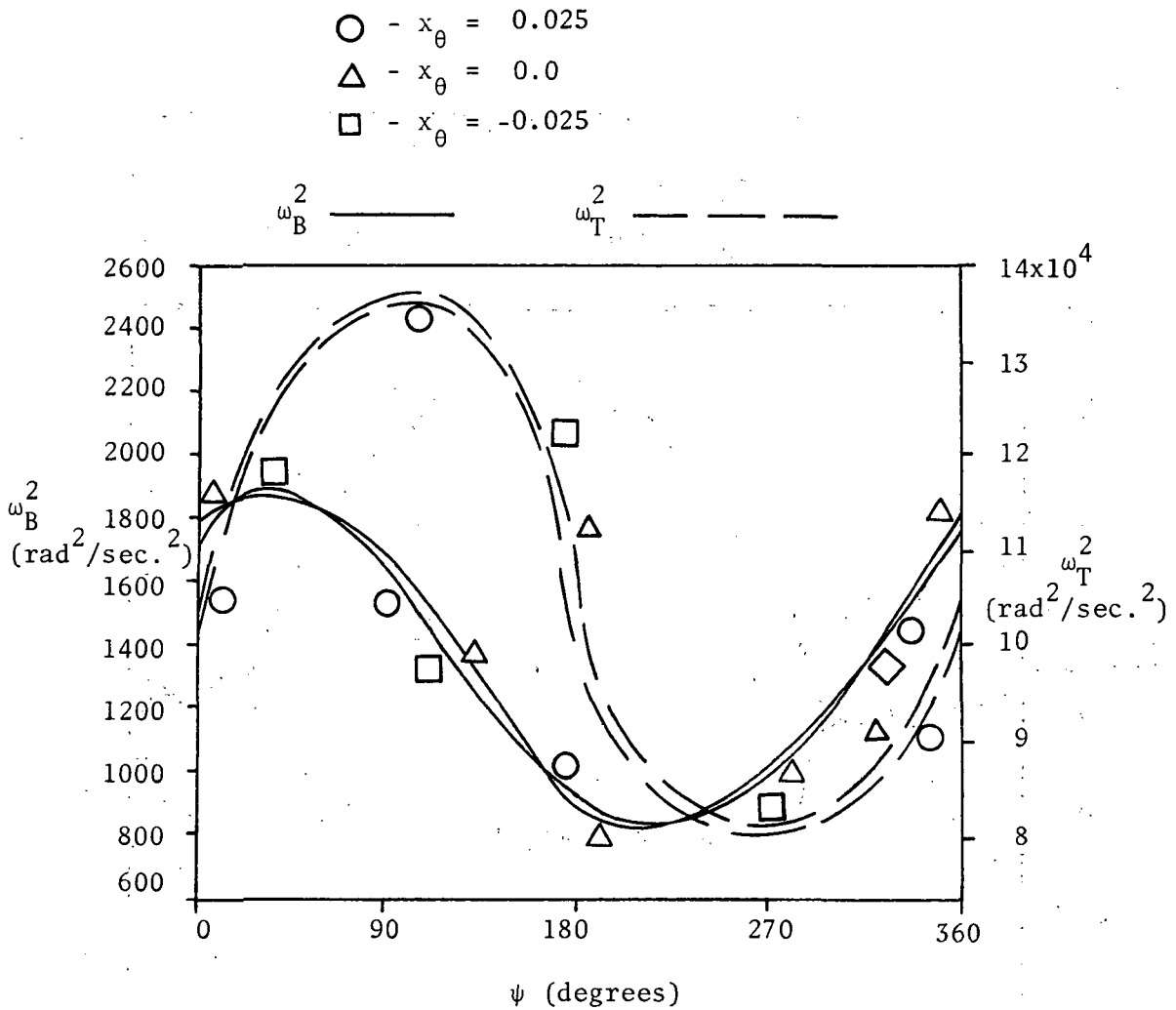
Fig. 34 Variation of Natural Bending and Torsional Frequencies with Blade Azimuth Positions for Various Eccentricities between Elastic and Mass Axes, $(\mu = 0.22, \kappa = 0.4)$.
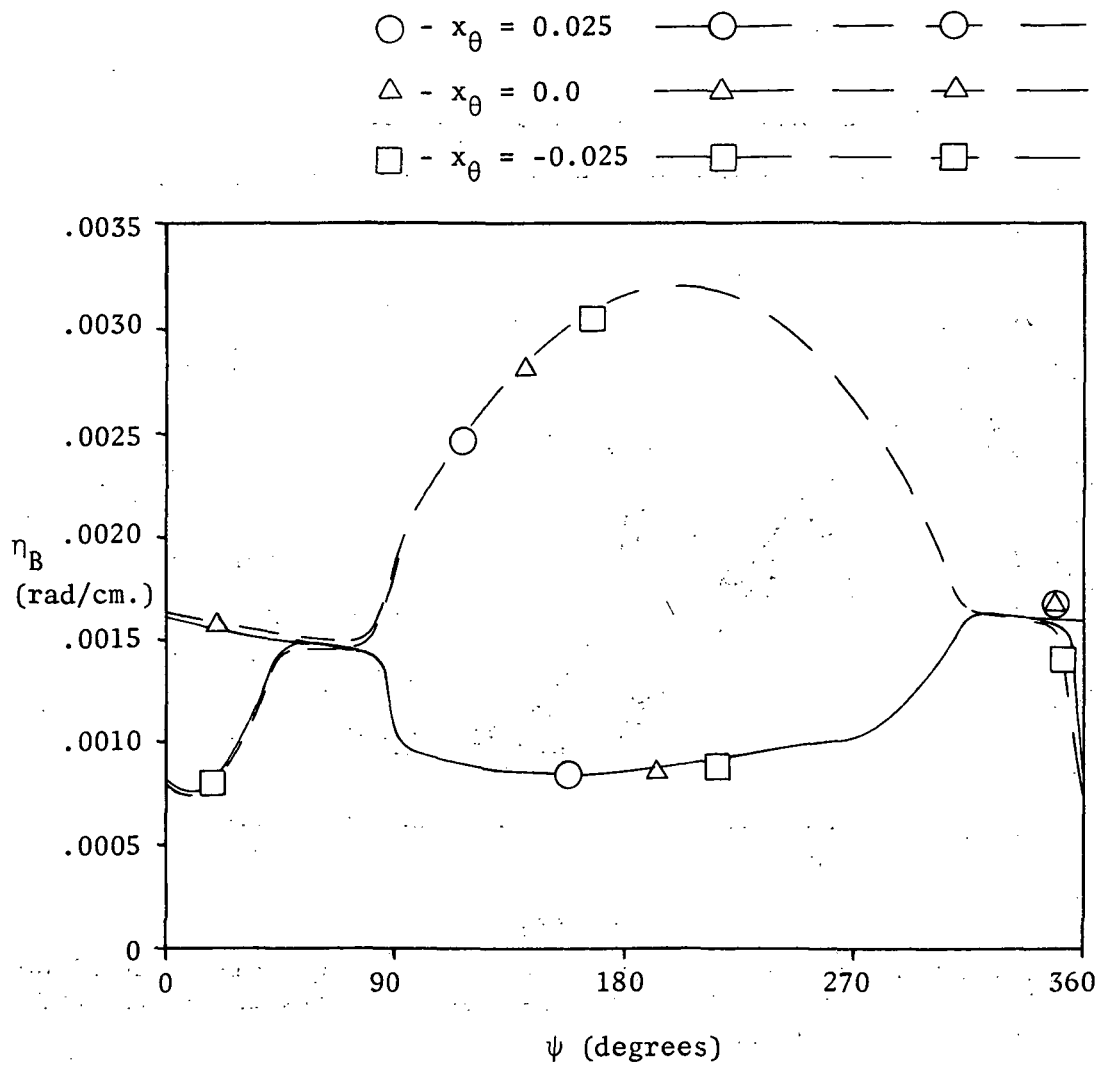
Fig. 35 Variation of Coupling Ratios for the Bending Mode with Blade
Azimuth Positions for Various Eccentricities between Elastic
and Mass Axes, ($\mu = 0.22$, $\kappa = 0.4$).

"The aeronautical and space activities of the United States shall be conducted so as to contribute . . . to the expansion of human knowledge of phenomena in the atmosphere and space. The Administration shall provide for the widest practicable and appropriate dissemination of information concerning its activities and the results thereof."
—NATIONAL AERONAUTICS AND SPACE ACT OF 1958

NASA SCIENTIFIC AND TECHNICAL PUBLICATIONS

TECHNICAL REPORTS: Scientific and technical information considered important, complete, and a lasting contribution to existing knowledge.

TECHNICAL NOTES: Information less broad in scope but nevertheless of importance as a contribution to existing knowledge.

TECHNICAL MEMORANDUMS: Information receiving limited distribution because of preliminary data, security classification, or other reasons. Also includes conference proceedings with either limited or unlimited distribution.

CONTRACTOR REPORTS: Scientific and technical information generated under a NASA contract or grant and considered an important contribution to existing knowledge.

TECHNICAL TRANSLATIONS: Information published in a foreign language considered to merit NASA distribution in English.

SPECIAL PUBLICATIONS: Information derived from or of value to NASA activities. Publications include final reports of major projects, monographs, data compilations, handbooks, sourcebooks, and special bibliographies.

TECHNOLOGY UTILIZATION PUBLICATIONS: Information on technology used by NASA that may be of particular interest in commercial and other non-aerospace applications. Publications include Tech Briefs, Technology Utilization Reports and Technology Surveys.

Details on the availability of these publications may be obtained from:

SCIENTIFIC AND TECHNICAL INFORMATION OFFICE

NATIONAL AERONAUTICS AND SPACE ADMINISTRATION
Washington, D.C. 20546